LUND UNIVERSITY
Faculty of Science

MASTER OF SCIENCE
DISSERTATION

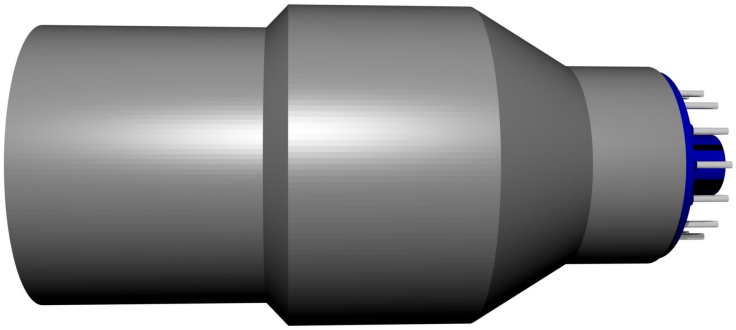

Using the $LaBr_3$:Ce scintillation detector for mobile γ-spectrometry

Author:
Jonas NILSSON

Supervisors:
Robert FINCK
Peder KOCK
Christer SAMUELSSON

Department of Medical Radiation Physics

November 16, 2010

Abstract

When doing mobile γ-spectrometry the equipment has for several decades been limited to NaI(Tl) and Ge-based detectors. Recent developements has led to a possible replacement of NaI(Tl)-based systems in the form of a new scintillation material: $LaBr_3$:Ce (cerium doped lanthanum bromide). $LaBr_3$:Ce-detectors successfully compete with NaI(Tl)-based detectors when considering resolution, efficiency, and decay time of the scintillation light. Its only main drawback is the fact that it is internally contaminated. The detector crystal contains a small percentage of the radioactive isotope ^{138}La as well as ^{227}Ac, which places the $LaBr_3$:Ce-detector at a disadvantage in comparison to NaI(Tl)-detectors, when measuring low photon fluences.

Several methods for compensating for the internal contamination are explored in this thesis. Two of those methods were found to work well for usage in a static measurement setup and a mobile setup respectively.

The problem of energy calibration drift, caused by temperature change and other causes, is also explored as this is a cause for concern when doing background compensation. Furthermore, a test to study if it is possible to use the $LaBr_3$:Ce-detector in a multi-detector system has been done with positive results.

Contents

1 Introduction

It could be argued that the most important discovery in γ-spectrometry is the discovery of NaI(Tl) as a scintillation detector material. Scintillation materials used in γ-spectrometry emit short pulses of electromagnetic radiation in the visible to ultraviolet light region when ionising radiation is absorbed. To measure the amplitude or pulse height of these light pulses, a photo multiplier (PM) tube is used. The PM-tube first converts the light photons to electrons and then amplifies the resulting current by accelerating them into a chain of so-called dynodes at which the electrons are multiplied as the kinetic energy of the electrons is converted to more electrons with lower kinetic energy. At the end of the dynode chain, the current is measured with the appropriate electronics. NaI(Tl) has relatively good properties for a scintillation material and has thus served as one of the main workhorses for the γ-spectrometry community for over 60 years [1, 2]. Although high resolution HPGe detectors have now replaced NaI(Tl)-detectors in the laboratory, NaI(Tl) is still the go to material when it comes to sensitivity and is for this reason still widely used in the mobile gamma spectrometry role.

Despite extensive research, an alternative to NaI(Tl) as a scintillation material, which addresses several of its problems (resolution, linearity, efficiency, and decay time) at once has not been found until very recently [3, 4].

An alternative, was found in the form of $LaBr_3$:Ce [5]. In 2001 van Loef *et al.* was able to produce a small $LaBr_3$:Ce-crystal and found that its properties as a scintillation crystal for radiation detection was superior to that of NaI(Tl). A limiting factor using $LaBr_3$:Ce is that naturally occurring lanthanum contains a small fraction (0.09 %) of ^{138}La, which is radioactive with a half-life of $1.1 \cdot 10^{11}$ years [6]. Lanthanum is also chemically similar to ^{227}Ac, which is also mined together with lanthanum and has a half-life of 21.8 years. This results in an always present background, which is not related to the measured radiation field .

The focus of this thesis was to examine the properties of a 3"x 3" $LaBr_3$:Ce-detector for use in a mobile setup, which involved studying how to best take advantage of the strength of the detector while if possible avoiding its weaknesses. This included the development of a method for compensating for the internal contamination of ^{138}La and ^{227}Ac, which inhibits the systems ability to detect low levels of radiation. There was also some focus on finding out if the detector is usable for future multi-detector mobile γ-detector systems.

1.1 Background

The first $LaBr_3$:Ce-crystal produced and characterized for use in γ-spectrometry [5] was found to have a greater light yield and better energy resolution than NaI(Tl) (see Table 1). Furthermore, decay time of the scintillation light was almost an order of magnitude shorter (Table 1) as compared to NaI. Density of the $LaBr_3$:Ce-crystal was also found by van Loef *et al.* to be greater than to that of NaI(Tl) (Table 1).

Table 1: Important properties of $LaBr_3$:Ce (from van Loef *et al.* [5]) and NaI(Tl) (from Sakai *et al.* and Knoll [7, 3]).

	$LaBr_3$:Ce	NaI(Tl)
Light yield (photons / MeV)	$61 \cdot 10^3$	$\sim 40 \cdot 10^3$
Energy resolution at 661.7 keV (%)	2.85	≈ 7
Decay time (ns)	35	230
Density (g/cm^3)	5.29	3.67

The energy linearity of a $LaBr_3$:Ce crystal (0.5 % Ce) was studied and it was found to be superior to NaI(Tl) [8]. The resolution and the effect that cerium-concentration had on light yield and decay time was also investigated, although these results were refuted by later research [9].

NaI(Tl)-detectors are well known for their unstable energy calibration when the temperature is changing [10]. For this reason Moszynski *et al.* and Bizarri *et al.* studied the effect of temperature on light yield and decay time on $LaBr_3$:Ce-crystals [11, 12]. Their results showed that the effect is relatively small. When considering the whole detector however, the effect of temperature on energy calibration can be large [11, 13]. Moszynski *et al.* attributed this to the effect of temperature on the PM tube.

Small amounts of ^{138}La and ^{227}Ac can be found in the $LaBr_3$:Ce-detector and several articles have reported on how they affect the pulse height distribution when performing spectrometry with a $LaBr_3$:Ce-crystal [14,15,16,17]. ^{138}La has two decay modes; $\beta-$ and electron capture with the end products ^{138}Ce and ^{138}Ba respectively. As the β-particle is absorbed in the crystal and therefore always detected, γ-photons are always detected in coincidence with β-particles which is why no gaussian γ-peaks can be seen originating from this decay-mode. If a γ-photon is completely absorbed in the detector at the same time as the β-particle, which in this case has a high probability, it will result in a shift of the β-continuum to a higher energy. Alternatively; the decay of ^{138}La through electron capture, registers as a multiplet in the pulse height distribution. This is the result of a single γ-energy with the added probability of absorption of an X-ray photon from the recently decayed atom.

At energies from 1.5 MeV to 3 MeV, it is possible to see several peaks that come from the decay of ^{227}Ac and its daughters through α-decay. Although these α-particles have a high energy (several MeV), the resulting peaks in the pulse height distribution are found at lower energy because the light yield from α-particles in the crystal is much lower than for γ and β-radiation. It was found by Nicolini *et al.* [16] that the position of the α-peaks in the pulse height distribution could be described by the equation:

$$E_\mathrm{r} = a + bE_\mathrm{a} \tag{1}$$

where E_r is the real energy of the α-particles, E_a is the apparent energy of the α -particles, a has the value 1.35 (MeV) and b has the value 2.36. The addition

of a is caused by the recoiling nuclei as well as the emission of several low energy γ and X-ray photons.

When studying the resolution of the $LaBr_3$:Ce-detector, it was found that the resolution was lower than NaI(Tl) at energies lower than 100 keV [18,19,20]. Dorenbos *et al.* hypothesised that surface effects contributes to the lower resolution at lower energies [20], though Balcerzyk *et al.* who studied similar problems with $LaCl_3$:Ce-crystals, found that surface effects is not a likely explanation for the lower resolution in $LaCl_3$:Ce below 100 keV [21]. Milbrath *et al.* suggests that loss in resolution in comparison to NaI(Tl) is caused by non-proportionality of the light yield in NaI(Tl)-crystals [19].

Because of the higher light yield from $LaBr_3$:Ce-crystals as well as the order of magnitude lower decay time of that light, the PM-tube must be able to handle much higher currents than is the case for PM-tubes coupled to NaI(Tl)-crystals [20]. Several articles [14, 20, 22] mention modifications done to existing systems to improve the linearity of detector systems, especially for higher γ-photon energies. Another alternative is to use PM-tubes with fewer dynodes [23].

2 Theory

2.1 Describing a γ-energy peak

As a large part of this work consist of analysing pulse height distributions, a model is needed which can describe a peak or several close peaks in a pulse height distribution along with the background under the peaks of interest. The following model can be used for that purpose:

$$R_n(n) = A + Bn + \sum_{j=1}^{k} C_j \exp\left(-\frac{(n-\mu_j)^2}{2\sigma_j^2}\right) \tag{2}$$

where R_n is the number of pulses in channel n, A and B describes the linear background, C_j is the amplitude of the Gaussian, μ_j is the centroid of the Gaussian and σ^2 is the variance.

2.2 Testing linearity

One of the many ways to test the linearity of a data set, is to calculate the correlation coefficient of the data points (also called Pearsons'r) [24]:

$$\rho = \frac{\mathrm{cov}(x,y)}{\sigma_x \sigma_y} \tag{3}$$

where x and y are the two variables and σ_x, σ_y are their respective standard deviations.

2.3 Detector resolution

The resolution of a γ-spectrometer at a certain energy is calculated with the following equation [3]:

$$R|_{\text{Poisson limit}} = \frac{\text{FWHM}}{H_0} \tag{4}$$

where $R|_{\text{Poisson limit}}$ is the resolution, FWHM is the full width at half maximum of a (gaussian) peak and H_0 is the centroid energy of that peak.

2.4 Simple energy calibration

If only two peaks are known, it is possible to do a simple energy-calibration by solving the following equation:

$$y = a + bx \tag{5}$$

where y in this case is the energy, x is the channel number a and b are the constants acquired when solving the equation.

2.5 Energy distribution of β-radiation

It is a well known fact that β-radiators radiates two particles when they decay. This makes the energy distribution between the three involved particles into a three particle problem. This means that β-radiation is not mono energetic. An equation which describes the energy distribution of the β-particles from a β^--radiator is the following [25].

$$N(T_e) = \frac{C}{c^5}\sqrt{T_e^2 + 2T_e m_e c^2}(Q - T_e)^2(T_e + m_e c^2) \tag{6}$$

where T_e represents β-particle energy, c is the speed of light, m_e is the electron mass, Q is the max energy of the β-particle and C is the amplitude of the distribution.

2.6 Detection limit

When performing any kind of γ-spectrometry of weak γ-sources, it is often desirable to know the limit at which these can be detected. Currie [26] has developed a framework for answering this question. In his article he also gives an example which can be used to calculate the detection limit of a γ-radiation detection system which will be summarised here.

There are two kinds of errors when determining if a radiation source is present or not:

1. The conclusion that there is a source present when in reality, there is not.
2. The conclusion that there is no source present when in fact there is.

In the example given by Currie, he sets the constraint that either of these cases should occur in at most 5 % of the cases studied. By also acknowledging that there is a background in the measurement, which can not be removed but is well known, he arrives at the following equation:

$$L_D = 2.71 + 4.65\sqrt{B} \tag{7}$$

where L_D is the the number of pulses, excluding the background pulses, needed to correctly decide if source is present in 95 % of the cases and B is the number of background pulses.

Intuitively, a source, if present, should always be detected if the measuring time is long enough. To decide how the time affects the value of L_D, Fink [27] extended Equation 7:

$$L_D = \frac{2.71 + 4.65\sqrt{B_{\text{cps}}t}}{t} \tag{8}$$

where t is the measuring time and B_{cps} is the number of background pulses per second measured.

3 Materials and methods

The $LaBr_3$:Ce-system used (SN: Q521CsB) consist of a ⌀76 x 76 mm^3 $LaBr_3$:Ce-crystal (5% Ce) grown by Saint-Gobain Crystals and coupled to a XP5700, 8 stage, Photonis produced PM-tube (SN: 221). The crystal with PM-tube, was connected to an ORTEC digiBASE MCA (SN: 09268063), which is a pre-amplifier, amplifier, analog-to-digital converter, multi channel analyser and high voltage supply contained in a small unit connected directly to the PM-tube. The final package was placed in a protective aluminium-cylinder of thickness 4.5 mm (see Figure 1).

The measurements were mainly done in a low-activity room with a background of 3 to 4 counts per second (cps) when measured with a 3" x 3" NaI(Tl)-detector placed in a protective aluminium cylinder.

Additional equipment is specified for each individual experiment.

Figure 1: $LaBr_3$:Ce-crystal in aluminium-tube with front cap removed.

3.1 Energy linearity of PM-tube

The relatively high currents in PM-tubes connected to $LaBr_3$:Ce-crystals (see Section 1.1), especially at higher γ-photon energies, has been reported to cause a loss in linearity of $LaBr_3$:Ce-detector systems. Some sources [28, 29] mention potential ways to alleviate this problem. The general idea is to lower the gain in the PM-tube by lowering the high voltage over the dynodes and thus decrease

the loss of energy linearity at higher currents. This loss in gain is compensated for by increasing the gain in the amplifier. The result should be an increase in energy linearity paid for in a slight loss in energy resolution.

It was confirmed that the high voltage could be dropped 100 V from (by the supplier recommended) 740 V, without changing the energy window (0-3000 keV) in the resulting pulse height distribution. Measurements were made with ^{137}Cs, ^{60}Co, ^{133}Ba as well as ^{22}Na point sources with the PM-tube set to both voltages. Measurements were not done in a low-activity environment though a measurement and subtraction of the background was performed. The measurement times were in the order of several minutes up to 1 hour.

The peak width was determined by fitting the model described in equation (2) to the peaks produced by the sources used. For most of the peaks used, k was set to 1 as those could be considered singlets. The peak from the ^{133}Ba-energy of 356 keV was instead considered to be a part of a multiplet of three energies (303, 356 and 384 keV) with k set to 3 for this case.

Curve-fitting was performed with a variant of the Levenberg-Marquardt curve fitting algorithm. And the uncertainty in these curve-fittings were calculated with the Jackknife algorithm described by Meinrath *et al.* [30].

Linearity was tested with equation 3 and resolution was calculated with equation 4.

3.2 Energy calibration drift

Because the system is to be used to compare measurements done hours or days apart, it is important to examine the drift in energy calibration.

Drift in energy calibration is a widely known problem for scintillator detectors and the consensus is that this is caused by temperature sensitivity in the detector. Although the effect temperature has on energy calibration of $LaBr_3$:Ce-detectors has already been studied to some degree, it was important to study the stability of this particular $LaBr_3$:Ce-detector. This aspect of the detector was investigated in several steps which will be explained in the following sections.

3.2.1 Stability at room-temperature

A test of the the energy calibration drift was performed in two separate experiments.

The first experiment was done on a relatively short time scale; a ^{137}Cs-source was placed ≈2 dm from the detector in a regular laboratory environment. The detector then made 1 minute live time measurements for almost 6 hours. A very simple energy calibration was performed with Equation 5. The two peaks used were the ^{137}Cs peak and the X-ray peak at 37 keV. Although it can be inaccurate to use only two peaks for energy calibration, the accuracy was considered enough in this case.

The second experiment was done on a time scale in the order of several days. The $LaBr_3$:Ce-detector was placed in a low-activity room and set to

make 15 minute measurements. 8 series of measurements were made. As no ^{137}Cs-source was used this time, the energy calibration had to be done with the internal contamination peaks. The peaks used were the the 37 keV X-ray peak and the ^{138}La multiplet. The method for energy calibration was the same as mentioned in the previous section with one exception; because a multiplet was used, k was set to 2 in Equation (2) when doing curve fitting.

It is possible to get an indication if energy calibration drift is caused by a change of gain in the detector or a change in the zero-point energy. This is tested by redoing the energy calibration, through Equation 5, for every single 15 minute measurement and studying how the value of b and a in that equation changes. A change in b should be caused by a change in gain whereas a change in a should be caused by a change in zero-point energy.

3.2.2 Stability at room-temperature with stabilisation-software

The digiBASE has the ability to stabilise the energy calibration by adjusting the gain and zero-point energy. For this to work, two peaks must be defined; preferably one peak at a low energy and one peak at a high energy. For this experiment, the X-ray peak (37 keV) from ^{138}Ce at the very beginning of the pulse height distribution and the ^{40}K/^{138}La multiplet around 1460 keV was used as stabilisation peaks.

The experiment was performed with two different basic conditions:

- A ^{137}Cs point source of $3 \cdot 10^5$ Bq was placed 2 dm from the front of the $LaBr_3$:Ce-detector and several pulse height distribution measurements were performed with live time[1] of 2 minutes. The experiment was conducted for more than 3 hours which resulted in 110 measurements.
- A ^{137}Cs point source of 37 ± 18 MBq was moved gradually closer to the detector with each measurement set to a live time of 5 minutes. All in all, pulse height distributions were measured at 22 points.

Both of these experiments were performed in a regular laboratory-environment.

To determine the centroid channel of the ^{137}Cs-peak from the obtained pulse height distributions, a method similar to the one described in Section 3.1 was used. The model was the one described in Equation (2) with k set to 1.

Energy calibration was performed through the use of Equation 5. The used peaks were the 37 keV X-ray peak and the 661.7 keV ^{137}Cs-peak.

3.2.3 Stability in a varying temperature environment

When doing mobile γ-spectrometry with scintillation detectors, a very real problem is the change in ambient temperature caused by the day-night cycle and changing weather. To test the effect of changing the temperature of the detector, the detector was placed in a refrigerator together with a temperature sensor as well as a small heater. A $3 \cdot 10^5$ Bq ^{137}Cs-source was also placed in the

[1] Live-time is defined as the amount of time that the detector is measuring radiation.

refrigerator to use as a reference point for energy calibration drift. See Figure 2. The stabilisation software was turned off for this experiment.

The experiment began with cooling of the detector to a little over the minimum allowed operational temperature (5°C). The detector was kept cool for a little more than 4 days to ensure that the whole detector reached thermal equilibrium. The refrigerator was then turned off and allowed to heat up to room-temperature. After one more day, this was in turn followed by further warming of the detector by turning on the heater. Finally, the heater was turned off and the refrigerator turned on again after another one and a half days.

The measurement time for each individual pulse height distribution was 15 minutes. Tracking of the centroid of the ^{137}Cs-peak in the pulse height distribution was done in the same way as previous energy calibration stability experiments, by fitting Equation (2) to the 661.7 keV peak of ^{137}Cs. No background correction was performed. A temperature sensor was attached to the detector and the temperature was logged every minute.

As in previous experiments, a simple energy calibration was performed with Equation (5) and the X-ray peak at 37 keV as well as the ^{137}Cs-peak at 661.7 keV. For every measurement, a temperature corresponding to that measurement was extracted from the temperature log.

3.2.4 Effects of the earth's magnetic field

The effect of the earth's magnetic field on the energy calibration of the detector should, according to some findings [28], not be underestimated. The earth's magnetic field mainly affects the PM-tube and if the effect is large enough, could potentially render the detector unusable for mobile γ-spectrometry. Because of the difficulty and time consuming effort of testing all the rotational degrees of freedom of the detector, the experiment was limited to showcasing a potential effect. The experiment was carried out by fixing a small ^{137}Cs source of 22 kBq to the front of the detector and then pointing the detector north, south, east and west with the carrying handle pointing upwards. This experiment was performed indoors in Lund, Sweden and the only measure taken to limit the effect of other magnetic fields was to use a compass and make sure that it pointed north in the area were the experiment took place.

A nickel iron alloy, called mu-metal, has the property of reducing magnetic fields. To test if a potential earth magnetic field effect could be limited with the use of mu-metal, the experiment described above was repeated with a sheet of mu-metal wrapped around the detector.

The same method as used in previous experiment, was also used here to analyse the energy calibration drift that the ^{137}Cs-peak underwent.

3.3 Internal contamination

The internal contamination is perhaps the greatest hurdle in using the $LaBr_3$:Ce-system to detect γ-radiation sources. The internal contamination must for this

Figure 2: The setup used to test energy calibration stability of the $LaBr_3$:Ce-detector when the temperature is changing.

reason be measured in a setting where the external background is negligible.

The internal contamination of the $LaBr_3$:Ce-detector consist of ^{138}La as well as ^{227}Ac including several daughter nuclides. To be able to use the detector, this internal radioactivity must be understood. The first step in this part is to make a measurement in a low-activity room where naturally existing radiation is low in comparison to the radiation with origin in the $LaBr_3$:Ce-detector. To obtain good statistics, this measurement was done over the course of several days. A problem introduced by long measurement times is the drift of the calibration. This was solved by the use of the stabilisation-function in the digiBASE and Gamma Vision software. To get a general idea of the background in the low-activity room, measurements were also done with a 3" x 3" NaI(Tl)-detector supplied by Teledyne (model S-1212-1).

Measurements were also done on the cosmic background radiation by decreasing the PMT-voltage to allow the $LaBr_3$:Ce detector to measure energies up to several MeV. The measurement of the cosmic background radiation made was done to estimate this influence to the pulse height distribution at the energy range of 0 to 3000 keV.

Because the half-life of ^{138}La is about 10^{11} years, it will not be possible to measure a change in the activity of this radionuclide during the lifetime of the $LaBr_3$: Ce-detector. The half-life of ^{227}Ac however, is only 21.7 years and its decay leads to a cascade of daughters, each with a different half-life. To calculate when equilibrium is reached between the production and decay of these daughters an array of first order differential eqations, which describes the decay and buildup of all the relevant nuclides, were created. This array of equations were then integrated over with a variation of the Livermore Solver for Ordinary Differential Equations [31] algorithm, with the starting condition that ^{227}Ac had one atom and all the other nuclides had zero atoms.

To ease analysis of the result, the number of nuclides was converted to activity and normalised to 1. Daughter nuclides with negligible activity were removed.

3.4 Modelling the internal contamination

When the internal background is known, it can be modelled and to some extent be compensated for. Three different methods for modelling (and compensating) for the internal background were explored.

3.4.1 Creating a function

If it is assumed that all the "structures" in a pulse height distribution can be modelled by simple mathematical equations, these equations can then be combined to model the complete pulse height distribution. The following equations were used in the modelling of the $LaBr_3$:Ce background pulse height distribution. Note that i represents the equation number in the combined model of the internal contamination.

The most important part of the model is the gaussian distribution which is widely used for modelling γ-radiation full energy peaks. For this case, the gaussian was reduced to the following equation:

$$R_{n,i}(n) = A_i \exp\left(-\frac{(n-\mu_i)^2}{2\sigma_i^2}\right) \tag{9}$$

where $R_{n,i}$ is the number of pulses in channel n which is represented by equation number i and A is the amplitude of the distribution, μ is the centroid, and σ^2 is the variance.

As ^{138}La can decay through the emission of a β-particle, a model of a β-continuum had to be used. Equation 6 was used for this purpose. The equation was modified to work with the concept of channels instead of actual energies, with the following result:

$$R_{n,i}(n) = \begin{cases} A_i\sqrt{n^2+2nB}(c_Q-n)^2(n+B) & \text{if } n < c_Q \\ 0 & \text{if } n \geq C \end{cases} \tag{10}$$

where $R_{n,i}$ is the number of pulses in channel n which is represented by equation number i, A is the amplitude of the continuum, B represents a constant which mirrors the importance of the electron mass in the β-decay and c_Q represents the channel at which the β-particle receives the most energy from the decay.

The equations given above, describes the most obvious structures in a pulse height distribution. Something that is more difficult to model is the case of scattered radiation. To simplify the modelling of this contributor to the pulse height distribution, the distribution was split into smaller parts where these continuums could be approximated relatively well to be of linear nature. The equation used to describe the scattered radiation was the following:

$$R_{n,i}(n) = \begin{cases} a+bn & \text{if } n_{\text{low}} < n < n_{\text{high}} \\ 0 & \text{if } n < n_{\text{low}} \text{ or } n > n_{\text{high}} \end{cases} \tag{11}$$

where $R_{n,i}$ represents the number of pulses in channel n represented by equation number i, a and b represents the linear approximation, and n_{low} and n_{high} is the lower and upper limits to the application of the linear approximation as a model of the pulse height distribution.

The final model is constructed by adding as many instances as needed of Equation (9, 10, 11) together to as accurately as possible describe the internal contamination. This is done with the following equation:

$$R_n(n) = \sum_{i=1}^{j} R_{n,i}(n) \tag{12}$$

By making estimates of the parameters used in the complete model and then performing curve fitting of the model to the data, a better model of the background was acquired.

3.4.2 Interpolating measurement

The most basic way of compensating for the background when doing γ-spectrometry is to make a background measurement followed by measuring the sample and then subtracting the first measurement from the second. This only works if the energy calibration and resolution is unchanged between the two measurements. It is possible to make a slight modification to this procedure and compensate for changing energy calibration. If the calibration for both measurements is known, an interpolation-function can be created which approximates the number of pulses between two channels. This makes it possible to change the calibration of a measurement without actually making a new measurement of the internal contamination.

This method has its obvious downsides:

- It is impossible to change the resolution. If the resolution changes between the two measurements, this will result in an overshoot or undershoot in the measurement close to peaks.
- The number of pulses per channel in the re-calibrated measurement has to be changed to reflect a real measurement done with that energy calibration.
- If the difference in original energy calibration between the two measurements is large, the peaks in the re-calibrated measurement will be deformed. This effect will be larger for narrow peaks.

3.4.3 Using a spectrum

Because of physical limits, a radiation field can not be measured exactly. The limiting factors in γ-spectrometry is mainly efficiency and resolution. The actual radiation field has a spectrum of γ-photon energies, which when measured results in a pulse height distribution, where each and every γ-photon detected is registered to have an energy which falls into a probability distribution decided by the actual energy of the γ-photon. This probability distribution is the detectors resolution at that energy and a function which describes how that distribution changes over the detectors entire energy range, is the detectors transfer function. If the spectrum from the internal radiation as well as the transfer function is known, the internal radiation can be modelled perfectly. Though as mentioned earlier; the spectrum can not be measured, but the transfer function can be. By knowing the transfer function and the pulse height distribution, it is possible to calculate the spectrum through deconvolution. The problem with deconvolution of a γ pulse height distribution is that the transfer function varies in a non linear way with energy, which means that the distribution can not be properly deconvoluted through analytical methods and instead numerical algorithms must be used.

The method used in this thesis is not mathematically correct considering the problems with deconvoluting a γ pulse height distribution but should serve as

a demonstration of what is possible if proper deconvolution is performed. The algorithm is as follows:

1. Take a small set of channels at the beginning of the pulse height distribution.
2. Create a model of that data consisting of a gaussian with a width based on its position (energy).
3. Perform a fit of that model to the data.
4. If the fit is not "good enough"; add another gaussian to the previously mentioned model.
5. Add one channel to the data-set.
6. Go to step 3 and repeat until the whole pulse height distribution is covered.

The gaussian used can be found in Equation (2), with $A = B = 0$ and $k = 1$.

Based on what the criteria for "good enough" are, a more or less obvious pattern of overlapping gaussians can be observed in the final model. Because of the simple criteria used in this demonstration, the parameters of the criteria had to be different for different energy-ranges of the background measurement. This necessitated that the fitted gaussians for the different energy ranges were manually spliced together.

The deconvoluted pulse height distribution should reasonably well represent the true spectrum when considering γ-energy where every channel represents one energy. Because the transfer function (resolution) of the detector is already known, the deconvoluted spectrum can be used to create an accurate background pulse height distribution of the internal contamination, irrespective of how the gain or high-voltage is set.

Because of limits with the method described here, this example had to be tested on an energy range more limited than previous methods.

3.5 Scintillation response

If the $LaBr_3$:Ce-system is to be used to detect the direction to a point source, the scintillation response of the detector must be known or to be more specific: it must vary as little as possible for γ-photons absorbed by different parts of the crystal.

The angular response was tested in three stages explained in turn. The source used was a small piece of absorbent paper containing ~ 50 MBq $^{99}\mathrm{Tc}^{\mathrm{m}}$. The source was placed on a Rose's metal ingot, 70 mm high, with a hole 1.5 mm across bored through it, thus producing a narrow beam of 141 keV photons from the source. The ingot was in turn placed on a mechanism that allowed the movement of the ingot in all three axes with precision of 0.01 mm (Figure 3). All measurements were done with the crystal inside the protective aluminium cylinder.

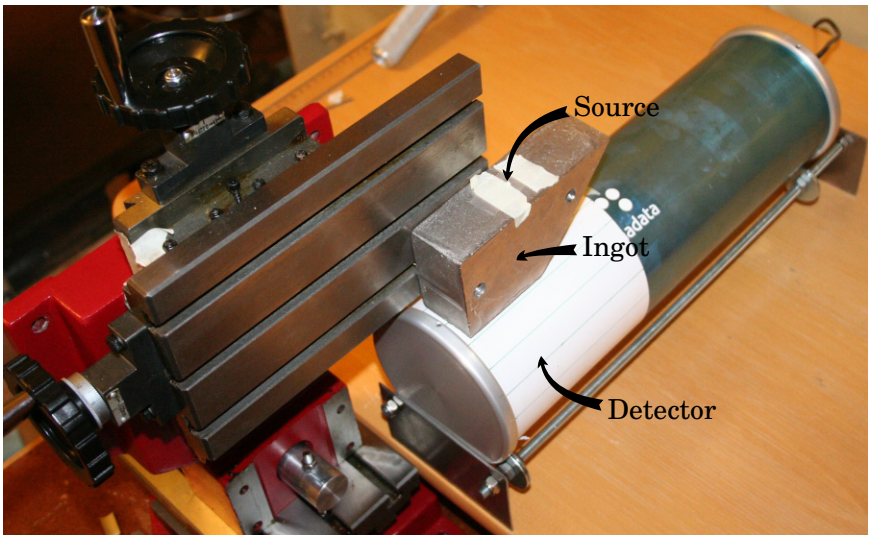

Figure 3: The setup used in the experiments described in Section 3.5.

3.5.1 The length of the crystal

As a test of the measurement system mentioned above, the response along one line of the crystal was tested at an interval of 2 mm. For every point measured, the measurement time was set so as to ensure at least 10^4 pulses in the full energy peak of 141 keV. The experiment was done with two different $^{99}\mathrm{Tc}^{\mathrm{m}}$ sources (of $\sim$ 10 MBq and $\sim$50 MBq) to test that the experiment was reproducible.

To figure out the detector response, the model described in Equation (2), with k set to 1, was fitted to a few channels around the full energy peak for every measurement. With the fitting complete, the parameter C (the amplitude of the gaussian) could then be plotted as a function of the ingot position when that particular pulse height distribution was measured. This was done based on the assumption that the resolution did not change between measurements. Because of the short half-life of $^{99}\mathrm{Tc}^{\mathrm{m}}$, the result had to be decay corrected. To approximate the uncertainty in C, the Jackknife algorithm as described by Meinrath *et al.* was used [30].

3.5.2 Homogeneity of the scintillation response

The homogeneity in the γ-photon response of the crystal was tested in two steps: the front surface and the cylinder surface. This was done by moving the same ingot with $^{99}\mathrm{Tc}^{\mathrm{m}}$-source as mentioned earlier, relative to the surface of the detector in appropriate steps. The step length used was 6 mm which resulted in 154 measurement points.

When checking the cylinder surface of the detector measurements were done along lines parallel to the detector and separated by 20°. There were 4 mea-

surement points for every one of those lines which resulted in 72 measurement points.

The resulting data was analysed as mentioned in Section 3.5.1. To visualise the result, the results were normalised to 1. These values were then fed to an interpolation algorithm which gridded the data and mapped it to a colour map.

3.6 Detector efficiency

$LaBr_3$:Ce-detectors mainly compete with NaI(Tl)-detectors which is why it is interesting to compare the absolute efficiency of the $LaBr_3$:Ce detector to that of a NaI(Tl)-detector with similar crystal dimensions (3" x 3"). As the $LaBr_3$:Ce-crystal has a higher density, it should have a higher efficiency.

The efficiency of the $LaBr_3$:Ce-detector was tested with small calibration-sources placed 106 cm away from the front of the detector. To obtain more accurate results, background correction was performed. Measurement time was on the order of tens of minutes to two hours depending on the activity of the γ-source.

The measurement of the efficiency of a NaI(Tl)-detector was done under less than ideal conditions when compared to the same measurements done with the $LaBr_3$:Ce detector. These measurements were done with the source only 25 cm from the front of the detector in a regular room. Furthermore, whereas the crystal of the $LaBr_3$:Ce-detector is enclosed in a 4.5 mm thick aluminium cylinder, the crystal of the NaI(Tl)-detector used was only encased in a thin aluminium casing. The NaI(Tl)-detector used in this experiment was supplied by Harshaw/Filtrol (model CP-488).

The equation used to calculate the efficiency is the following:

$$\epsilon = \frac{4\pi d^2 R}{n_\gamma S_{\text{det}}} \underbrace{\left(A(0) e^{-\lambda t} \cdot e^{\frac{\mu}{\rho}\rho d} \right)^{-1}}_{\mathscr{A}} \tag{13}$$

where d is the distance between detector and source, R is pulses per second representing a specific γ-energy from that source detected by the detector, n_γ is the photon emission probability of that specific γ-energy and S_{det} is the surface-area of the detector front. The part denoted with $\mathscr{A}$ compensates for the decay of the calibration-source since it was produced as well as the interaction of γ-photons in the air between the detector and the source. The $LaBr_3$:Ce-detector had an additional part which compensated for the aluminium casing.

The point sources used were ^{241}Am, ^{133}Ba, ^{137}Cs, ^{60}Co and ^{22}Na. The activity of these sources were in the range of 100 to 400 kBq with an uncertainty in activity of 3 %.

3.7 Energy linearity

To be able to properly use any of the background compensation methods described in Section 3.4, the energy calibration and energy linearity (or lack thereof) of the detector must be well known for both the measurement which is

Table 2: γ-photon energies and isotopes used in the energy calibration of the $LaBr_3$:Ce-detector.

Isotope	Energy (keV)		Isotope	Energy (keV)
^{22}Na	1275		^{133}Ba	81.00
^{24}Na	1369			276.4
	2754			302.9
^{40}K	1461			356.0
^{55}Co	477.2			383.8
	931.3		^{137}Cs	661.7
^{57}Co	122.1		^{207}Bi	569.7
^{60}Co	1173			1064
	1332		^{214}Bi	1765
^{89}Zr	909.2		^{241}Am	59.54

to be compensated as well as the measurement which is used to compensate for the internal contamination. It would be favourable to the validity of the experiment if several γ-photon energies could be used. The isotopes used are shown in Table 2. Because of previously mentioned stability problems (see Section 3.2), the measurements were done without any stabilisation. Instead, every measurement was manually adjusted to fit a pre-selected background measurement. The background was then subtracted from these measurements. Although this was crude and is a source of artefacts if there is a large enough difference in energy calibration between the two measurements, the method was deemed precise enough for this experiment. The final step was to fit the model described by Equation (2) to individual peaks ($k = 1$ in Equation (2)) or in a few cases, to multiplets ($k > 1$) in the pulse height distributions.

3.8 Energy resolution

The last background compensation method described (Section 3.4.3) does not only need a energy calibration but also a resolution calibration to create the transfer function used. The method used for determining the resolution is exactly the same as for the experiment described in the previous section and was in fact done at the same time with the same nuclides.

Resolution was calculated by extracting the standard deviation (σ) from the model (Equation (2)) fitted to the peaks and converting those values to resolution through Equation (4).

3.9 Measuring the internal contamination with a NaI(Tl)-detector

Because a future goal for the detector is to be used in a multidetector system together with several NaI(Tl)-detectors, it should be tested if the internal con-

tamination of the $LaBr_3$:Ce-detector has a big impact on the measurements of a NaI(Tl)-detector placed in contact with the $LaBr_3$:Ce-detector. Possible γ-photon energies detected by the NaI(Tl)-detector should include the 789 keV photon emitted when ^{138}La decays into ^{138}Ce and the 1436 keV photon emitted when ^{138}La decays into ^{138}Ba. The NaI(Tl)-detector used was of size 3" x 3" and enclosed in a protective aluminium tube.

The experiment was performed in a low-activity room with the NaI(Tl)-detector, made by Teledyne (model S-1212-1), at first placed alone in the room to measure background, followed by a measurement done with the $LaBr_3$:Ce-crystal placed as close as possible to the NaI(Tl)-crystal without removing either from their aluminium casings. Measurement time was 20 minutes.

3.10 Sensitivity of the $LaBr_3$:Ce-detector in mobile γ-spectrometry

Because of the goal of using the $LaBr_3$:Ce-detector in mobile γ-spectrometry, a comparison to existing detector systems should be made to see if there is any benefit in using this detector instead of more proven technology. Although car borne γ-spectrometry is often performed with large NaI(Tl)-detectors (4 liter volume is common), it is not reasonable to compare those detectors to a 3" x 3" $LaBr_3$:Ce-detector. Instead the comparison was made between the $LaBr_3$:Ce-detector and a 3" x 3" NaI(Tl)-detector.

For this purpose, Equation 8 was used. Although this equation is defined for a number of pulses, it can be extended to cover the number of pulses in an energy range of a pulse height distribution. As a full energy peak in a γ-ray pulse height distribution is a gaussian, the energy range used was one that covered 95 % ($\pm 2\sigma$) of the area of the peak at the current energy.

The comparison was made based on an indoor background measurement in Lund with a pulse rate from the $LaBr_3$:Ce-detector of ~890 cps and a pulse rate from the NaI(Tl)-detector of ~350 cps. The NaI(Tl)-detector used, was one built by Teledyne (model S-1212-1). As measurement time in mobile γ-spectrometry is usually set to 1 second, so as to achieve good spatial resolution in the measurements, t in Equation (8) was also set to 1 second. Detector efficiencies used were obtained from the experiment that produced Figure 23 whereas the used resolution was that from Figure 25. Resolution of the NaI(Tl)-detector were obtained from an article by Milbrath *et al.* [19]. Because those resolution measurements only cover an energy range of ~60-662 keV, the comparison between the two detectors were also limited to this range.

The two detectors compared are of the same size but has different efficiencies which can be seen in Figure 23. By doing linear interpolation and extrapolation of the efficiencies for the whole energy range, an actual comparison between the detectors can be made by dividing L_D with detector efficiency at the current energy.

3.11 Comparison of $LaBr_3$:Ce and NaI(Tl) detector measuring background radiation

To visualise the difference in sensitivity between the $LaBr_3$:Ce-detector and 3" x 3" NaI(Tl)-detector (supplied by Teledyne, model S-1212-1) two measurements were made with both:

- A stationary background measurement.
- A mobile γ-spectrometry measurement of a ^{137}Cs-source.

The stationary measurements were made indoors, in an environment which gave $\sim$ 350 cps in the NaI(Tl)-detector and $\sim$ 890 cps in the $LaBr_3$:Ce-detector. The measurements were made for 9 and 15 hours. No background correction was performed in this case.

The mobile measurement was made on Revinge heath outside of Lund, Sweden. The detector was placed in a car which drove along a straight gravel road at a speed of around 35 km/h. A ^{137}Cs-source with an activity of 37$\pm$18 MBq was placed at a distance of 20-30 m from the road. The measurement time was set to 1 second. The result from this drive-by was presented in a "waterfall display". The waterfall display data in three dimension where x-axis is time, y-axis is energy and the colour coding represents detector response.

An alternative to the standard waterfall display is the "deviation display" [32] which display positive changes in intensity. The data as represented by a deviation display can be seen in Figure 30.

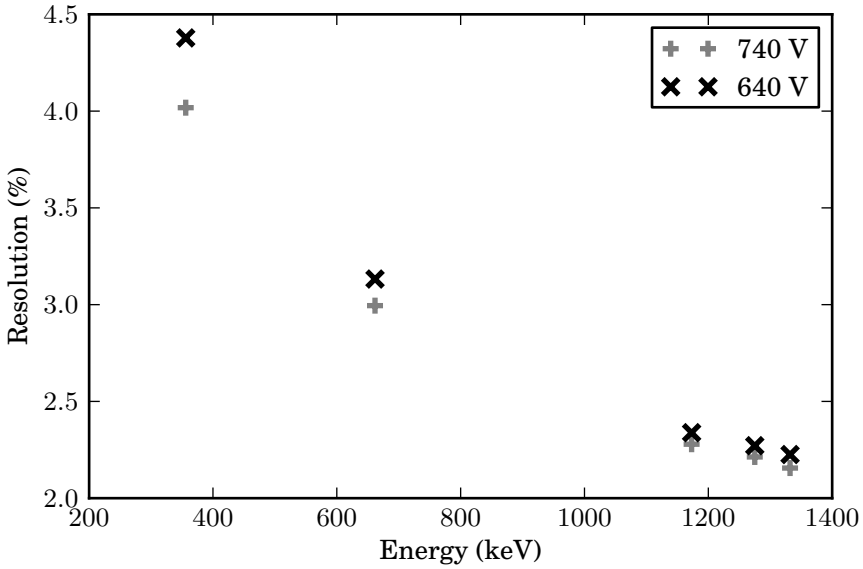

Figure 4: The resolution in percent as a function of γ-photon energy for two voltages used on the $LaBr_3$:Ce-detector. Note that the resolution is worse for the lower voltage and energy as fewer electrons are collected in the PM-tube. Uncertainty was found to be no larger than the symbols in the figure.

4 Results & Discussion

4.1 Energy linearity of PM-tube

The loss in resolution when lowering the voltage fed to the PM-tube can be seen in Figure 4. The uncertainties in the calculation of the energy resolution were found to be, at most, no larger than the symbols in the figure. Errors in the energy calibration were ignored. The result of calculating Pearson's r (Equation (3)) on the channel number versus energy was the following: both potentials gave a value of $\rho > 0.999$.

The figure shows that there was a clear loss in resolution as the PM-tube voltage was decreased, which was exactly as expected. Pearson's r shows that linearity for the energies tested was excellent and although Pearson's r was slightly higher for 640 V (not shown), the difference was insignificant.

The conclusion was that the potential small loss in linearity can be accepted, but the loss in resolution can not, which is why it is recommended that the PM-tube is fed the higher voltage. It is possible that higher resolution can be achieved if the voltage is increased above the recommended 740 V. Even if this result in a significant loss in linearity, this can be compensated for with a better and non-linear energy calibration.

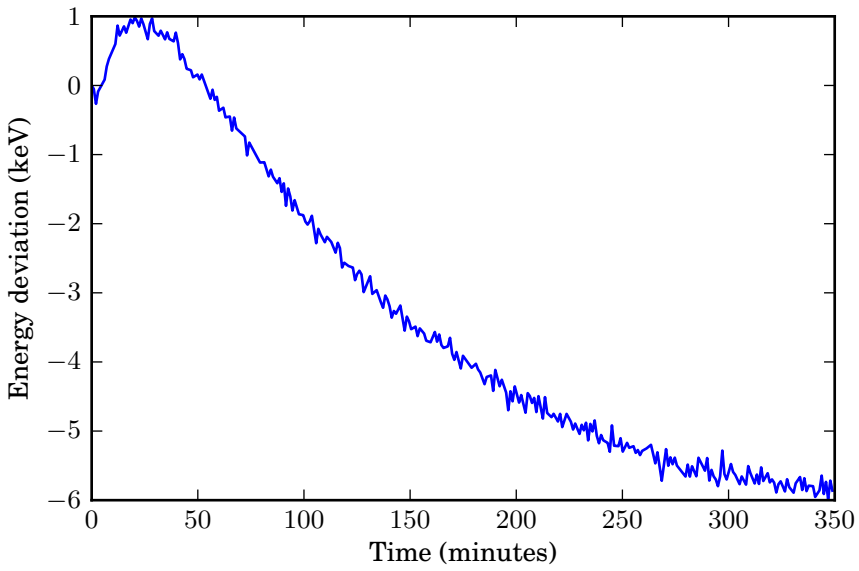

Figure 5: Energy calibration drift of a 661.7 keV ^{137}Cs-peak when the detector is at room temperature.

4.2 Energy calibration drift

4.2.1 Stability at room-temperature

Figure 5 describes energy calibration stability of the $LaBr_3$:Ce-detector on a short time-scale.

The result of the energy calibration drift, on a long time scale, of the lowest energy part of the multiplet can be seen in Figure 6.

Figure 7 shows how the variable a in Equation (5) changes if a new energy calibration is made for every measurement in the second experiment.

It was expected that the drift would be towards higher energy as the components were heated by their use and therefore produced a higher gain. As is shown, this did not hold true for the short time-scale (Figure 5) but did so for the long time-scale (Figure 6). The reason for this is so far unknown as the detector was expected to reach thermal equilibrium after at least a few days of use. Further testing has to be done if an explanation for the decrease in gain in the short term and the increase in gain in the long term is to be found.

There was some question as to what really caused the channel shift but Figure 7 strongly indicates that the energy drift comes from a change in gain and not a change in the zero-point energy, at least in a low-activity environment. It is expected that some zero-point shift would occur in an environment containing high levels of radiation because of afterglow in the crystal. If this is not the case or if that effect is negligible, then the problem with zero point shift encountered in Section 4.2.2 can be removed by simply not using zero-point stabilisation.

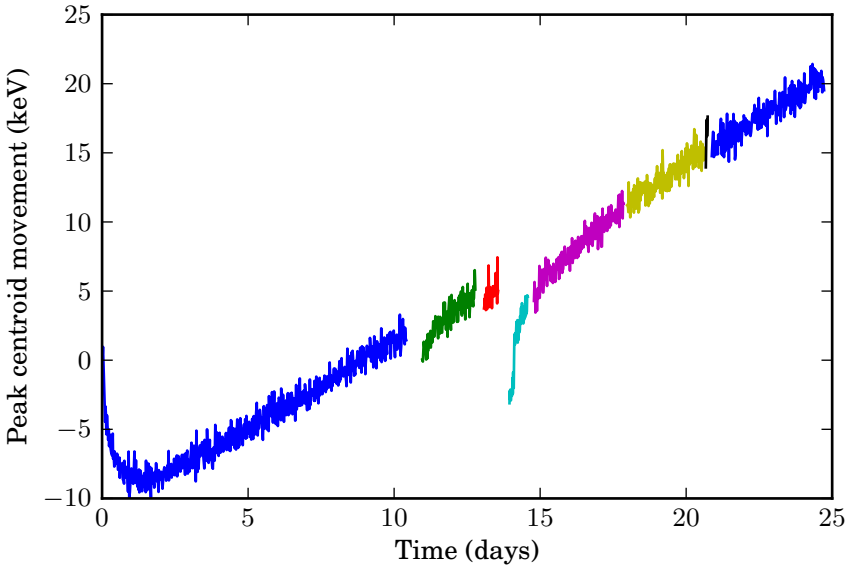

Figure 6: Energy calibration drift for the 1436 keV ^{138}La-peak. Note that as this experiment ran for several days, measurements were split into 8 series. Between these series, energy calibration measurements of different nuclides were performed. The fluctuations seen in the figure is produced by relatively short measurement times.

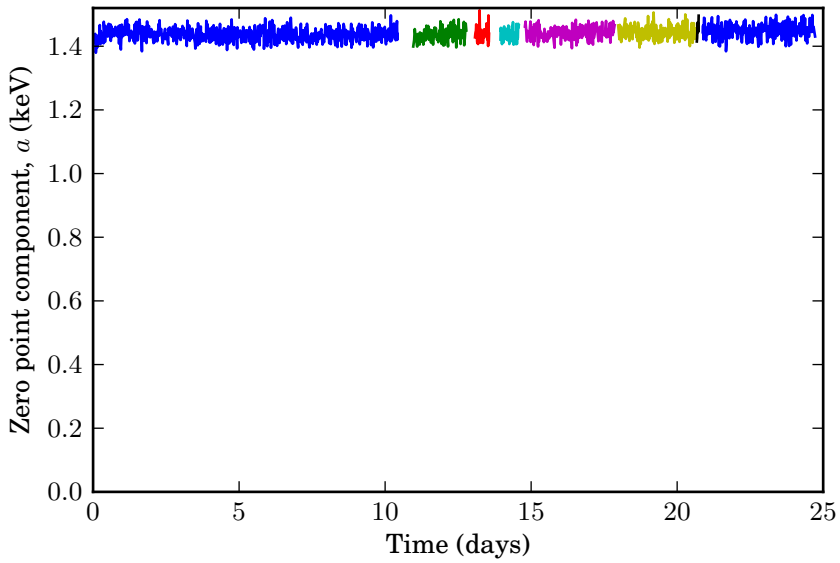

Figure 7: The zero point (channel zero) part (a) of Equation (5). Figure was created by performing an energy calibration of every measurement represented in Figure 6. The fluctuations are caused by the relatively short measurement times.

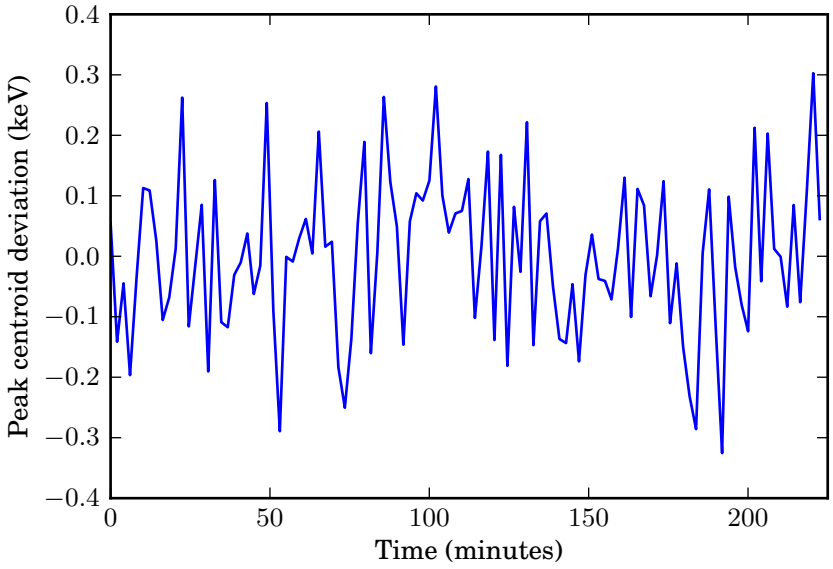

Figure 8: An indication on how well the stabilisation function of the digiBASE performs when measuring a static ^{137}Cs-source.

It can be seen at the very beginning of Figure 7 that there is a slight increase of a in Equation (5). This can possibly be explained by a contaminant in the low-activity room that gradually disappeared over the first 2-3 days of that measurement series. As this contaminant produced a low-energy peak at higher energy than that of the X-ray peak in the pulse height distribution, it most likely pushed the X-ray peak ever so slightly towards lower energy.

As mentioned in Section 3.2.1, the experiment consisted of 8 measurement series. This was because a more exact energy calibration was performed between these series. As can be seen in Figure 7, at the beginning of series 2 and 4, this appears to have affected the energy calibration drift. The energy calibration was at these points performed with calibration sources of strength up to a few MBq, which appears to have affected the energy calibration drift towards lower energy for relatively short amounts of time after the energy calibration measurements. Any reason as to why is so far unknown.

4.2.2 Stability at room-temperature with stabilisation-software

Figure 8 shows how the stabilisation function of the digiBASE performs when measuring a static ^{137}Cs-source. Specifically, the deviation from the mean centroid-energy for the ^{137}Cs-peak is shown.

The result from the second experiment, is presented in Figure 9. As this experiment is considered to showcase the problem with energy stabilisation,

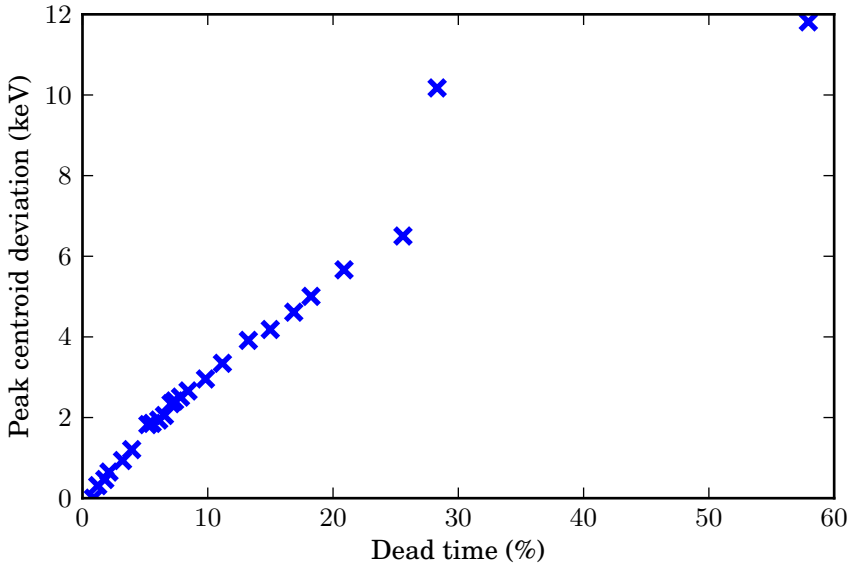

Figure 9: When measuring a non static ^{137}Cs-source, the stabilisation function of the digiBASE can not keep the energy calibration stable as shown in this figure. The outlier was probably caused by an experimental error. Because of the position of this outlier, it was not warranted to repeat the experiment.

drift in keV from the minimum energy is plotted against dead time[2].

When the radiation spectrum that the $LaBr_3$:Ce-detector measures is relatively constant, the stabilisation-function in the digiBASE perform well, as can be seen in Figure 8. When the radiation field was changing, the stabilisation function had a harder time to keep up as is evident by Figure 9. The reason for this can probably be attributed to the fact that as the ^{137}Cs-source was moved closer to the detector, the X-ray peak at the low energy end of the pulse height distribution was increasingly masked and shifted by scattered radiation. As the X-ray peak was used by the stabilisation function as a zero-point reference, this resulted in an overshoot where low-energy pulses were moved to the high-energy end of the pulse height distribution by the stabilisation function.

It could be argued that the problem described in the previous sentence will probably not present itself as a problem when doing mobile γ-spectrometry as the radiation-field is unlikely to be of such intensity as to mask the X-ray peak under normal conditions. What is likely to change during mobile γ-spectrometry however, is the amount of ^{40}K in the background, which will change the shape of the ^{40}K/^{138}La multiplet. As the stabilisation function of the digiBASE makes the assumption that a peak has a shape that can be approximated as gaussian-distribution, this change in ^{40}K activity will cause a drift in energy calibration.

[2]Dead time is a quantity often expressed in percent that reflects how large part of the the time actually passed (as opposed to live time) that the detector is unable to detect radiation.

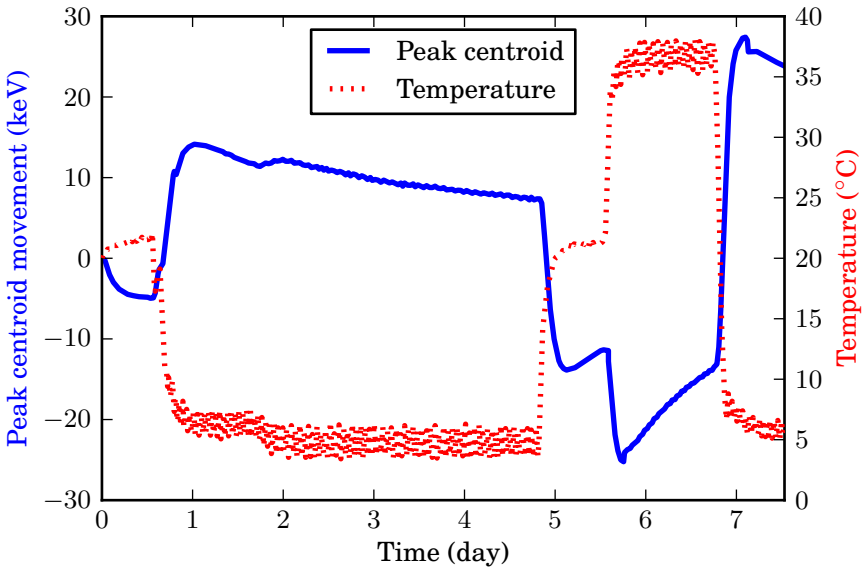

Figure 10: The energy calibration of the $LaBr_3$:Ce-detector is influenced by temperature change when the stabilisation function of the digiBASE is not used. The γ-photon energy used in this experiment was the 661.7 peak from ^{137}Cs.

The solution to this problem is to use a peak model which takes into account the fact that while the contribution of the internal contamination to the ^{40}K/^{138}La multiplet is basically constant, the contribution from ^{40}K is not. This is in fact the method used by $LaBr_3$:Ce-detectors employed by the Finnish Radiation and Nuclear Safety Authority [28].

4.2.3 Stability in a varying temperature environment

Figure 10 shows deviation in keV together with the temperature.

As mentioned in Section 1.1 of this text, the effect of temperature on the light yield in the $LaBr_3$:Ce-crystal should be quite small. When studying Figure 10, it is obvious that temperature has a very noticeable effect on the whole detector.

It can be clearly discerned from Figure 10 that the change in gain from change in temperature has at least two components: One relatively quick component that decreases gain as the temperature increases and one very slow component that increases gain as temperature is increased. Moszynski *et al.* [11] mentions how the gain decreased in the PM-tubes they used as temperature was increased. This can probably explain the quick component seen in Figure 10.

Both Moszynski *et al.* as well as Bizarri *et al.* [11,12] show that light output increases with temperature for the $LaBr_3$:Ce-detector at the temperature range used in this experiment. This effect is according to Moszynski *et al.* on the order of 0.01%/°C and could therefore possibly explain the slow component observed in Figure 10.

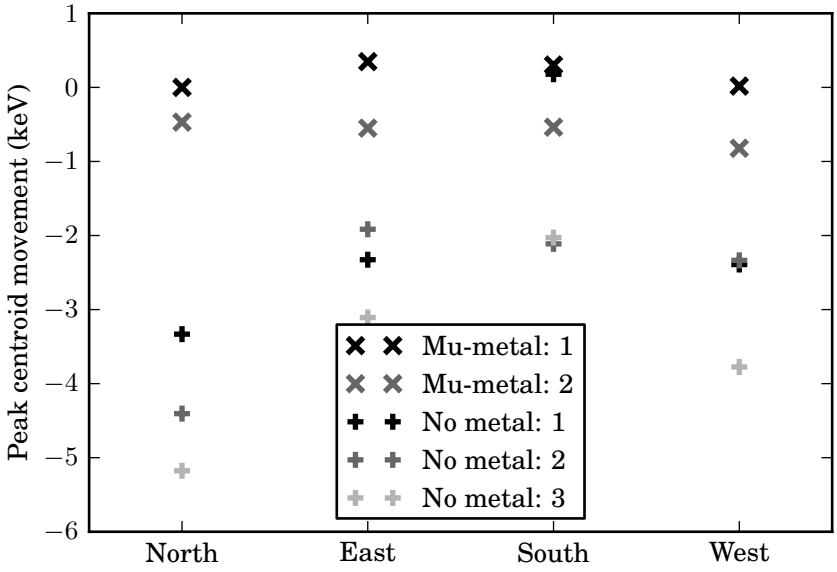

Figure 11: Effect on energy calibration of pointing the front of the $LaBr_3$:Ce-detector into the four cardinal directions. The experiment was repeated two times when using a magnetic field shielding metal (mu-metal 1 & 2) and three times without.

Although ambient temperature appears to be a big factor in changing the energy calibration of the $LaBr_3$:Ce-detector, other causes should not be ruled out. One other possible explanation is that a change in ambient humidity might affect the detector electronics. This should not be a major contributor to energy calibration drift in this particular detector though, as the aluminium tube containing the detector and its electronics, is hermetically sealed. Though this does not rule out a change in relative humidity as it is possible that water is trapped inside the aluminium tube, the change should only be related to the temperature of the detector.

4.2.4 Effects of the earth's magnetic field

The result from this measurement can be studied in Figure 11. The figure clearly shows an effect of the earths magnetic field on the energy calibration of the detector. It is also clear that the mu-metal shielding has some effect on reducing the drift caused by the earths magnetic field. Interestingly, although the results all appear to follow the same trend, there is a clear difference between the 5 measurement series. This can be explained by one or more of the following points:

- Although the table upon which experiment was made, was constructed mostly out of wood, the frame and legs were made out of metal. This

could have affected the magnetic field enough to make the placement of the detector on the table critical.

- It has already been established that there is a energy calibration drift which is time based. This drift was not compensated for.
- The outset of the experiment was to only point the detector at the four cardinal directions. In practice, the placement was not perfectly reproduced for all directions and the detector underwent some rotation around its other axes to.
- The mu-metal sheet did not cover the entire detector and the placement was changed between the measurement series.

Despite this, it is clear that the earths magnetic field has to be taken into account when using this detector. This is especially problematic when doing mobile γ-spectrometry as the change in the vector of the magnetic field relative to the detector can be very drastic in those circumstances.

When the previously mentioned experiment was performed, it was found that the magnets in the computer used to collect the data, also affected the detector from a few decimetres away. It is possible that magnetic fields of similar strength can be found in vehicles, though it is uncertain if their effect on the detector is relevant as they might be static. Either way, it is recommended that if the detector is to be used in mobile γ-spectrometry, it should be properly shielded by mu-metal.

4.3 Internal contamination

Figure 12 shows background measurement in a low-activity room made with a $LaBr_3$:Ce. Table 3 gives an explanation of what can be seen in this figure. Note that the energy intervals given in that table are approximate.

Measurement of the cosmic background-radiation (shown in Figure 13) indicates that this effect on the detector is negligible in comparison to the internal contamination of the $LaBr_3$:Ce-detector. If it is assumed that the amount of cosmic background radiation increase very little with decreasing energy, as indicated by the figure, the cosmic background can be approximated to induce less than 0.5 cps in the energy range of 0 - 3000 keV.

Although the measurement of the internal contamination in the $LaBr_3$:Ce crystal was done in low-activity room, it was recognised that the effect of other radiation-sources could not be eliminated completely. For this reason, a comparison measurement was done with a 3" x 3" NaI(Tl)-detector as can be seen in Figure 14. When comparing the $LaBr_3$:Ce and NaI(Tl) measurement, it is clear that the radiation in the room external to the $LaBr_3$:Ce-detector is negligible in comparison to the internal contamination. The NaI(Tl)-detector had a pulse rate of 3-4 cps whereas the pulse rate of the $LaBr_3$:Ce-detector was around 500 cps. If the incorrect assumption that most pulses registered by the NaI(Tl)-detector was of energies around 1.5 MeV is made, i.e. an energy where the

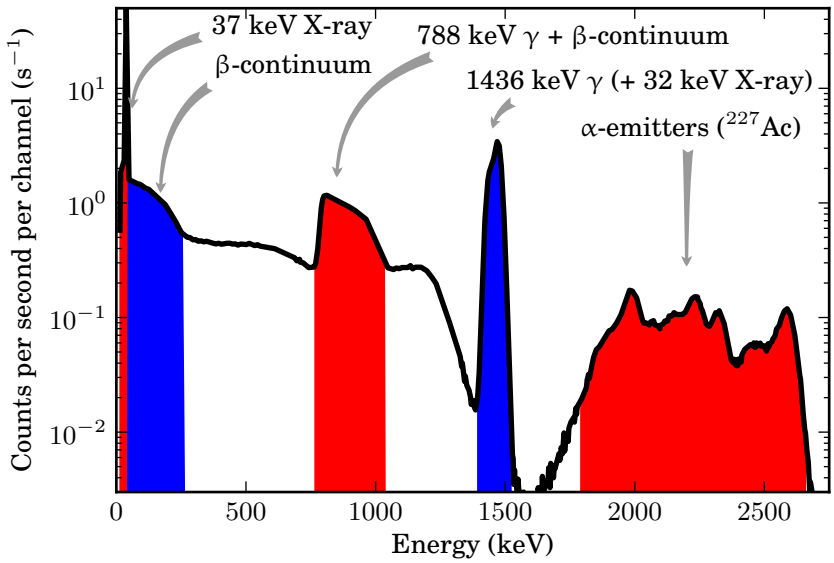

Figure 12: A pulse height distribution showing the internal contamination of the $LaBr_3$:Ce-detector along with an explanation of the more obvious features in the pulse height distribution. The measurement was made in a low-activity environment.

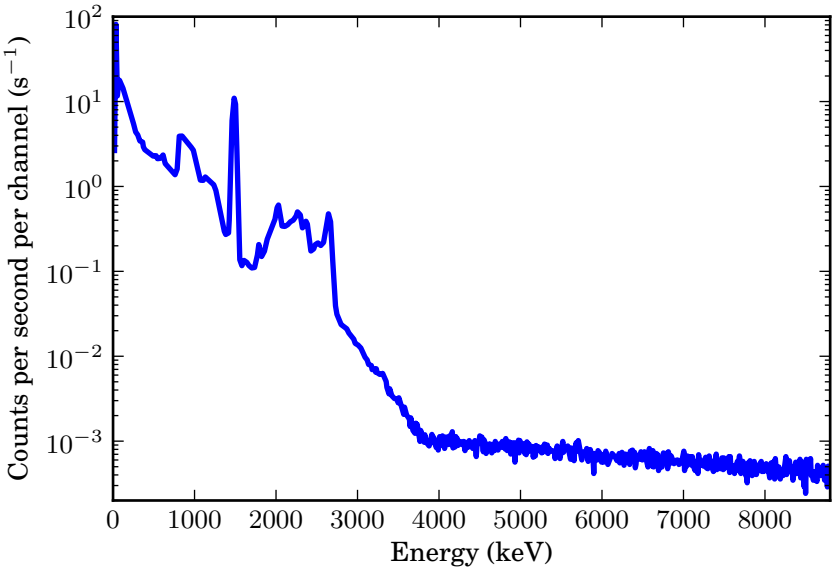

Figure 13: Measurement made with $LaBr_3$:Ce-detector which reveals cosmic background radiation at energies above 4 MeV.

Table 3: Explanation of the structures in a pulse height distribution from a $LaBr_3$:Ce-detector, caused by internal contamination.

Energy (keV)	Explanation
37	The first peak in the pulse height distribution comes from the emission of X-ray photons from ^{138}Ba after it has decayed from ^{138}La [28].
∼50-290	The continuum after the first peak comes from the absorption of a β-particle from the decay of ^{138}La into ^{138}Ce. As β-radiation is not mono-energetic, a continuum is created [16, 14, 15].
∼765-1050	When ^{138}La decays through β-decay to ^{138}Ce, there is a possibility that the 789 keV γ-photon is completely absorbed in the crystal. The resulting effect is that the β-continuum is shifted to a higher energy.
1436 & 1468	This multiplet-peak is the result of the decay of ^{138}La into ^{138}Ba. As this decay-mode has a very high probability of producing X-ray photons, the multiplet is an effect of the combination of 1436 keV photons and 32 keV X-ray photons [15, 18, 14, 29]. Note that although ^{40}K with its photon energy of 1461 keV is a part of the peak shown, the part is so small that it can for all intents and purposes be ignored.
∼1600-2750	According to several authors [15,17,19,21], the light yield of α-particles in the $LaBr_3$:Ce-crystal is much lower than for β-particles and γ-photons. This means that although the energy of the α-particles emitted from ^{227}Ac with daughters are in the order of several MeV, the peaks in the pulse height distribution appears in the energy range of 1.5 to 3.0 MeV.

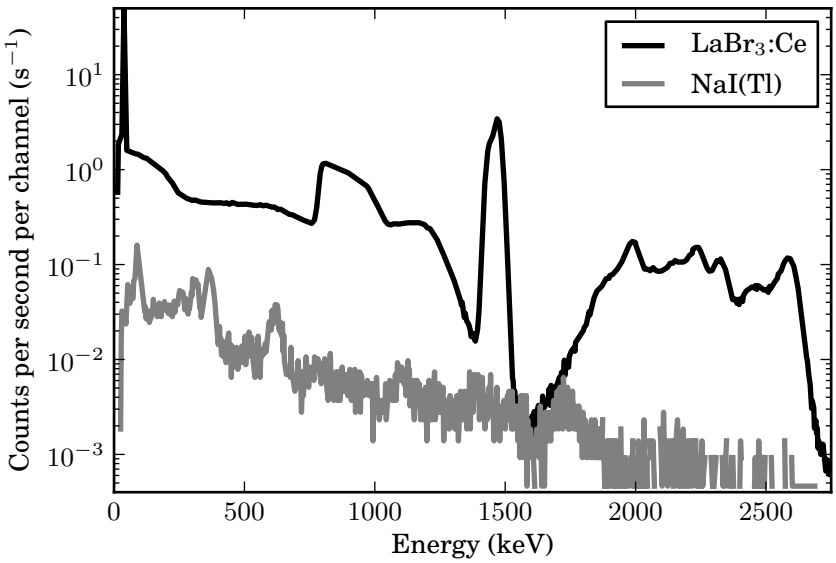

Figure 14: The same pulse height distribution measured with the $LaBr_3$:Ce-detector as shown in Figure 12 together with a measurement of the background in a the same low-activity environment with a NaI(Tl)-detector.

efficiency of the $LaBr_3$:Ce-detector is higher than that of the NaI(Tl)-detector and the difference in thickness of the aluminium casings has less importance. This would only amount to at most 10 cps from external sources when measuring with the $LaBr_3$:Ce-detector in the low-activity room, which still is negligible in comparison to the internal contamination.

The result of the calculation of the buildup of daughter nuclides can be seen in Figure 15.

4.4 Modelling the internal contamination

The model created from the instructions in Section 3.4.1, as well as the result of subtracting the model from a background measurement can be seen in Figure 16.

An example of the use of the algorithm described in Section 3.4.2 is shown in Figure 17.

The result of using the deconvolution described in Section 3.4.3 is shown in Figure 18. The result of a background correction using the method described in the same section,q is shown in Figure 19.

Of the three methods for background-correction tested, the least reliable appears to be the first one (Section 3.4.1), which uses a model of the internal contamination. One reason for this is that it is not mathematically sound to change the resolution of gaussians in the model. This results in over or undershot, if the resolution in the measurement on which the model is based, changes

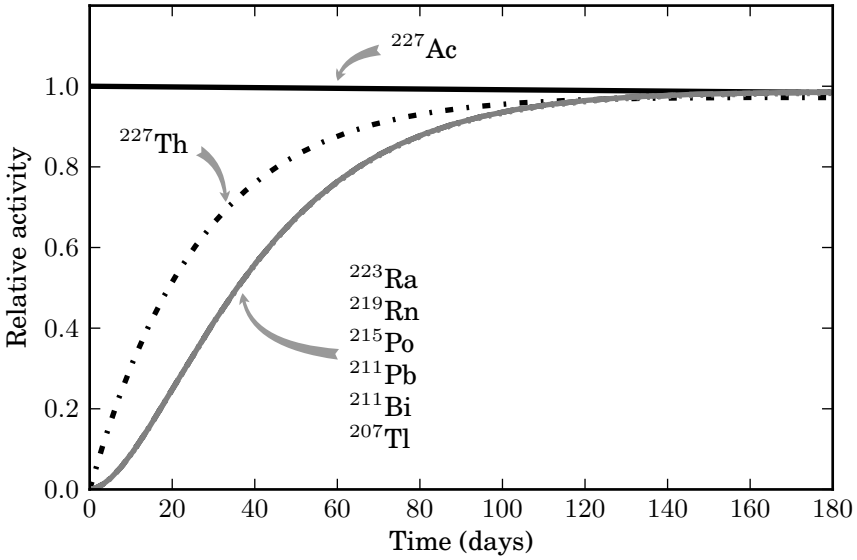

Figure 15: Theoretical calculation of buildup of activity of the daughter nuclides of ^{227}Ac. Note that daughters with very low-activity (because of very low yield) has been removed. The line representing ^{215}Po-activity overlaps the lines showing the activity of ^{223}Ra, ^{219}Rn, ^{215}Pb, ^{211}Bi and ^{207}Tl.

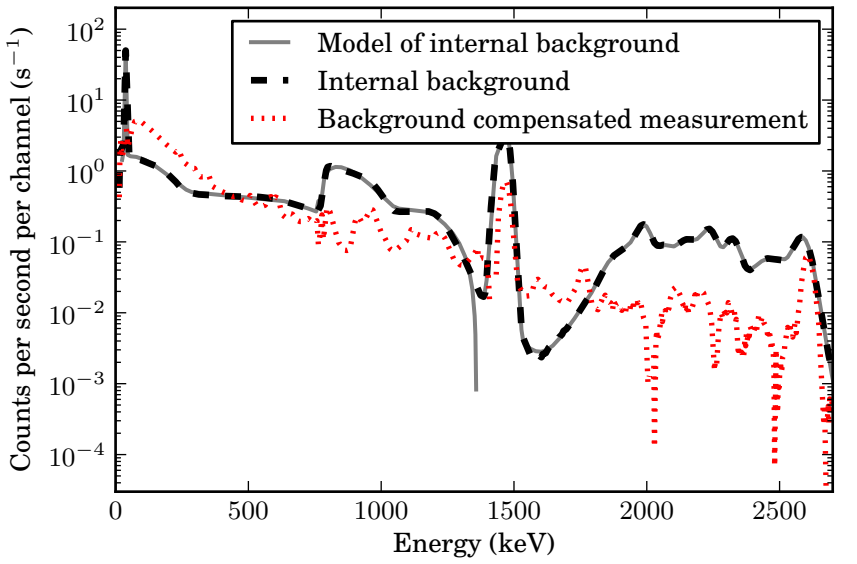

Figure 16: A model of the internal contamination of the $LaBr_3$:Ce-detector created from Equation (9, 10) and (11), as well as the result of using that model to subtract the internal background from a background measurement (the original measurement can be seen in Figure 17).

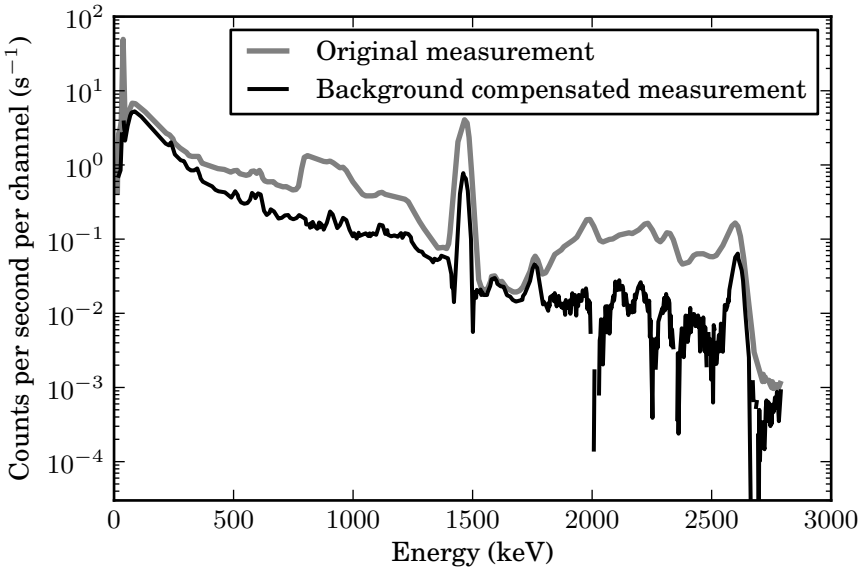

Figure 17: A background compensated pulse height distribution produced with the interpolation method described in Section 3.4.2 as well as the original measurement.

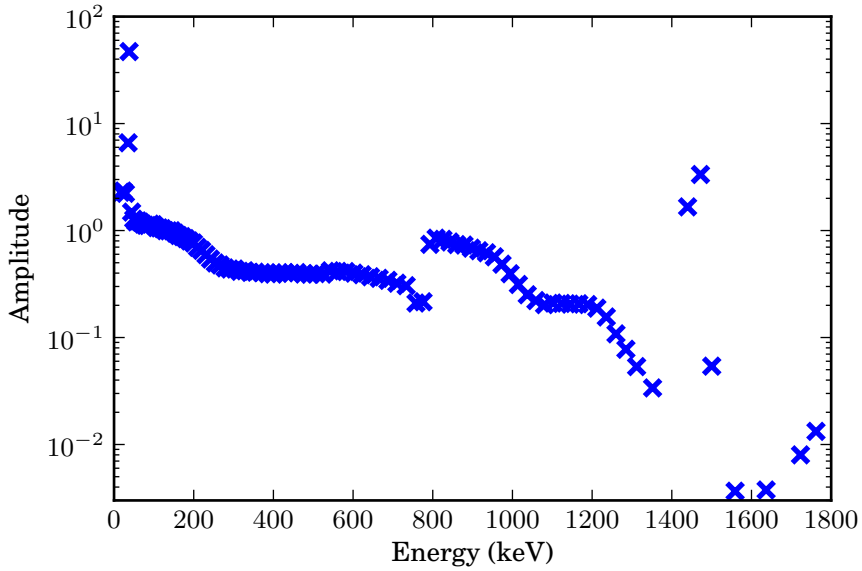

Figure 18: This figure gives energy and amplitude of the gaussians used to reproduce a pulse height distribution of the internal contamination of the $LaBr_3$:Ce-detector. The width of the gaussians, which is also needed, can be found in Figure 25. The gaussian used can be found in Equation (2), with $A = B = 0$ and $k = 1$. A description on the creation of this figure can be found in Section 3.4.3.

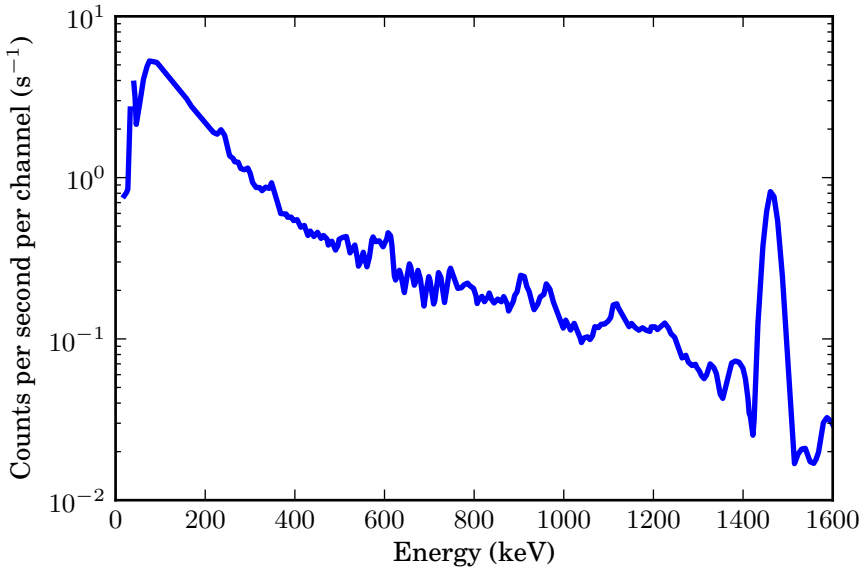

Figure 19: Background compensated pulse height distribution produced with the "spectrum"-method described in Section 3.4.3. Compare with Figure 16 and 17.

between the measurements of interest. Another problem is that it is hard do describe compton-distributions in the pulse height distribution. This leads to a model that does not quite represent the data upon which it is based. This is evident in Figure 16. Furthermore, changing the energy resolution, while possible, is cumbersome and this is made worse by the problem of modifying the amplitude of the model to reflect the total number of pulses given by the detectors internal radiation.

The second method, described in Section 3.4.2, while having the benefit of being easier to use than the first one, have the same problem when it comes to a change in resolution between measurements. This is evident in Figure 17 which show undershoot around high energy peaks. This method also has the problem of compensating for a change in the number of pulses per second.

Lastly, the method described which uses a deconvoluted background shows the most promise. As this method is based on using the transfer function of the detector, it can easily compensate for a change in energy calibration and resolution. The method also handles the number of pulses per second without any need for compensation. A case which this method will not handle as gracefully is a nonlinear change in energy calibration or resolution although none of the other methods will handle those cases either. The only big drawback is the problem in obtaining the transfer function as well as the deconvoluted background measurement. As mentioned earlier, the deconvolution algorithm used here needed a lot of hand holding and did not work at all in the α-peak area of the pulse

height distribution. Despite this, the problem should not be insurmountable. Figure 19 represents this method and has two obvious artefacts:

- Because of the imperfect deconvolution, individual gaussians which are not caused by any radionuclides, can be seen. This is most obvious in the 400 to 800 keV energy range.
- The background compensated X-ray peak has become negative. The reason for this is not entirely clear though other experiments have indicated that the count rate of some energy ranges is effected by the total count rate.

If background correction is to be widely used, it would be preferable if one method could be used on several different $LaBr_3$:Ce-detector systems without the need for measuring the transfer function and the background for every one. The prerequisites for this would be that:

- The amount of ^{138}La and ^{227}Ac is the same as in the detector from which the background measurement is obtained.
- The resolution is the same as the one in the detector used to obtain the transfer function.
- The shape and more importantly, the size is the same.
- ^{227}Ac has reached activity equilibrium with its daughters.

4.5 Scintillation response

The result of this experiment show no glaring inhomogeneity which would hinder the use of the detector in multi-detector location sensing system with reasonable accuracy. Especially considering other uncertainties in deciding location of a radioactive source, such as positioning errors and changing measurement geometry.

4.5.1 The length of the crystal

It can be seen from Figure 20 that the method used for measuring angular response by radiating the $LaBr_3$:Ce-crystal with a thin beam of radiation from a $^{99}Tc^{m}$ source is reproducible. It can be seen that although some points diverge noticeably from each other, the shape of the two series is the same. It is interesting to note that the sensitivity of the crystal is lower at the two ends than at the middle. There are a couple of possible explanations for this:

- Scintillation light that is produced closer to one edge of the crystal generally has to travel a longer distance before it hits the photocathode of the PM-tube. This increases the possibility that enough photons are lost that the pulse will appear outside the full energy peak in the pulse height distribution.

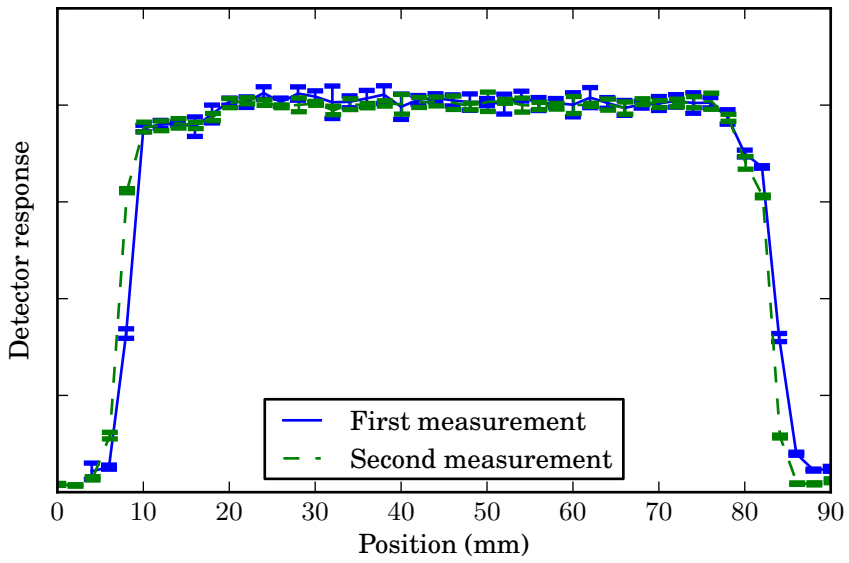

Figure 20: Detector response at 141 keV along the length of the $LaBr_3$:Ce-crystal. Note that the amplitude of the curves from the two experiments have been normalised.

- Because $LaBr_3$:Ce-crystals are grown much longer than the 76 mm of the crystal used in this experiment [33], they have to be cut into the correct size, it is possible that the cutting results in a slightly damaged crystal or that the cut surface reflects scintillation light slightly worse then an uncut surface.

In either case, the loss of sensitivity is noticeable but not dramatic and should not effect the usage of the crystal for its intended purpose.

4.5.2 Homogeneity of the scintillation response

The result of the this particular investigation is in the form of two figures that describe the homogeneity through a map. The front is described in Figure 21 whereas the cylinder surface response is shown in Figure 22. Note that in these figures, the blue dots indicate measurement points.

As can be seen in the figures, the scintillation response varies a few percent. The reason for this variation is not entirely clear and can possibly explained by experimental errors. Whatever the reason, the variation is small enough to not hinder the use of the detector in a multi-detector, direction sensing setup.

Though not shown here, the scintillation response of front of the detector was tested twice. The result not shown had a lower resolution than the one in Figure 21. The difference in scintillation response between the two measurements was negligible.

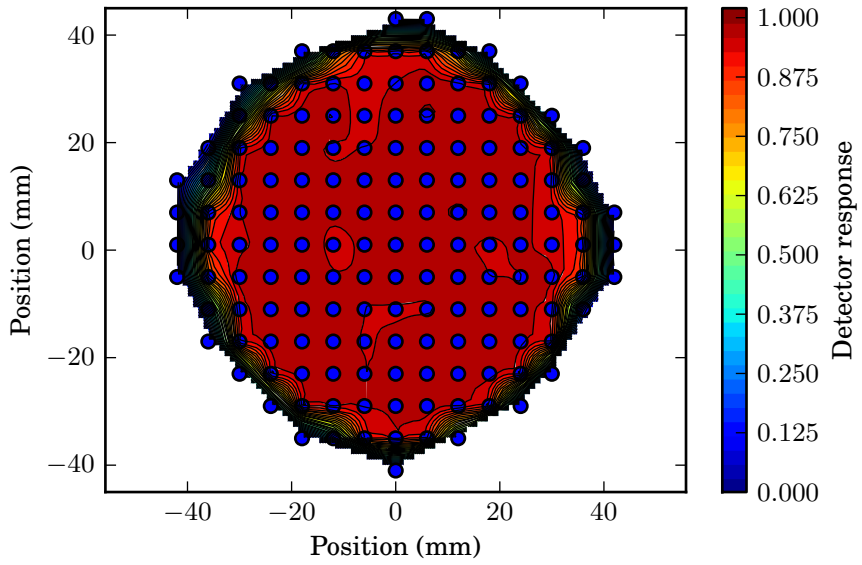

Figure 21: Scintillation response of the front of the $LaBr_3$:Ce-detector when using a γ-photon energy of 141 keV. Note that the blue dots represent measurement points.

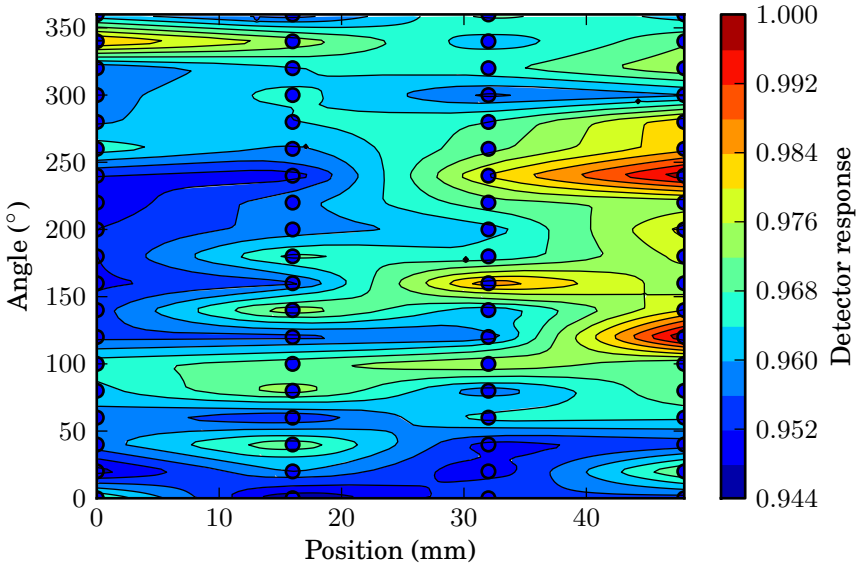

Figure 22: Scintillation response of the cylinder surface of the $LaBr_3$:Ce-detector when using a γ-photon energy of 141 keV. Note that the blue dots represent measurement points.

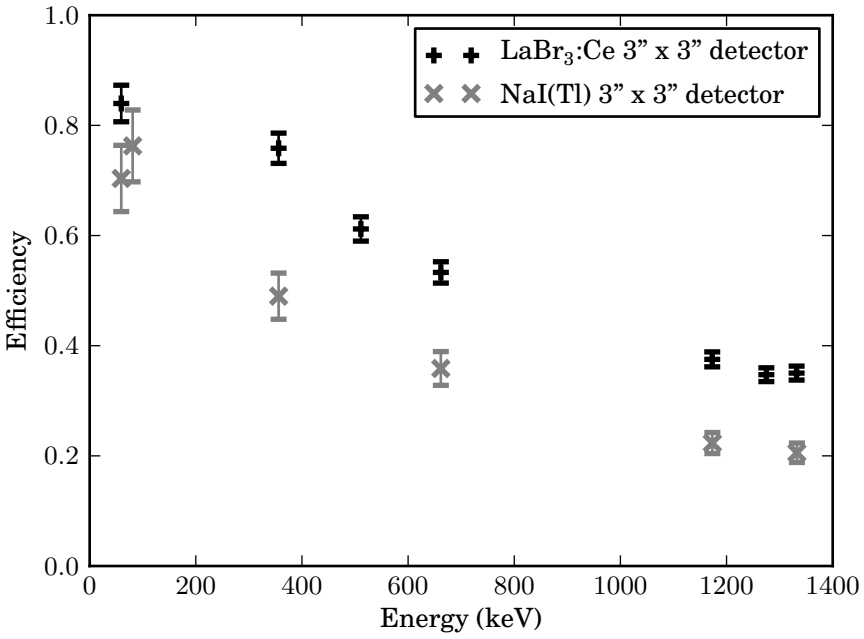

Figure 23: Absorbed photon per photon incident on the detector for the $LaBr_3$:Ce-detector and a 3” x 3” NaI(Tl)-detector. Measurements were made with the source placed so that the photons passed through the front of the crystal first.

4.6 Detector efficiency

The result of the comparison in efficiency between the $LaBr_3$:Ce-detector and a NaI(Tl)-detector can be seen in Figure 23. The y-axis is the probability that a photon of a given energy that passes through the front of the detector, undergoes complete absorption.

As is shown in the figure, the $LaBr_3$:Ce-detector consistently has a higher efficiency than the NaI(Tl)-detector over the tested energy range. Even though the absolute difference in efficiency is about the same over this range, the result is that the efficiency is almost twice as good at energies above 1100 keV. This difference can at least partly be explained by the higher density of $LaBr_3$:Ce.

4.7 Energy linearity

The result of the energy calibration can be seen in Figure 24 where energy is plotted against channel number for the specific background correction measurement used.

As hinted on in Section 3.1 and definitely shown in the figure, the energy linearity is excellent in comparison to a NaI(Tl)-detector which also has been reported earlier [14, 20, 22]. The assessment from these results is that for mobile

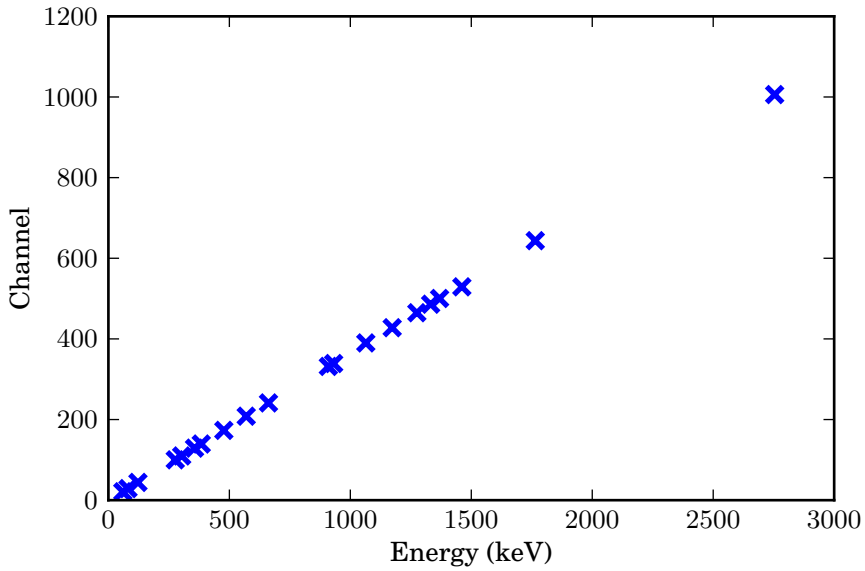

Figure 24: Energy calibration of the $LaBr_3$:Ce-detector.

γ-spectrometry, the coupling between between channel number in the pulse height distribution and energy, can very well be represented by a linear function.

4.8 Energy resolution

The energy resolution plotted against the γ-energy can be seen in Figure 25. An estimation of the uncertainty in the fit was calculated with the Jackknife algorithm described by Meinrath *et al* [30]. All but one of the resolution measurements were estimated to have an uncertainty of two to three orders of magnitude smaller then the calculated resolution.

The figure shows in accordance to what was mentioned in Table 1, that the resolution of the $LaBr_3$:Ce-detector is superior to the resolution of NaI(Tl)-detectors at 661.7 keV. As resolution data for NaI(Tl)-detectors was lacking, it could not be confirmed that the resolution of NaI(Tl)-detectors was better at energies lower than 100 keV.

The figure indicates that the resolution deviates from the general trend around 1460 keV. This is caused by imperfect background correction of the $^{138}La/^{40}K$ multiplet around that energy. Furthermore, the resolution at 661.7 keV has also been affected by an imperfect background correction and energy drift during measurement, caused by the fact that no energy stabilisation was used. The resolution shown in Figure 25 for 661.7 keV is 3.00 $\pm$0.01 %, whereas a resolution of 2.9 % has been achieved under better circumstances.

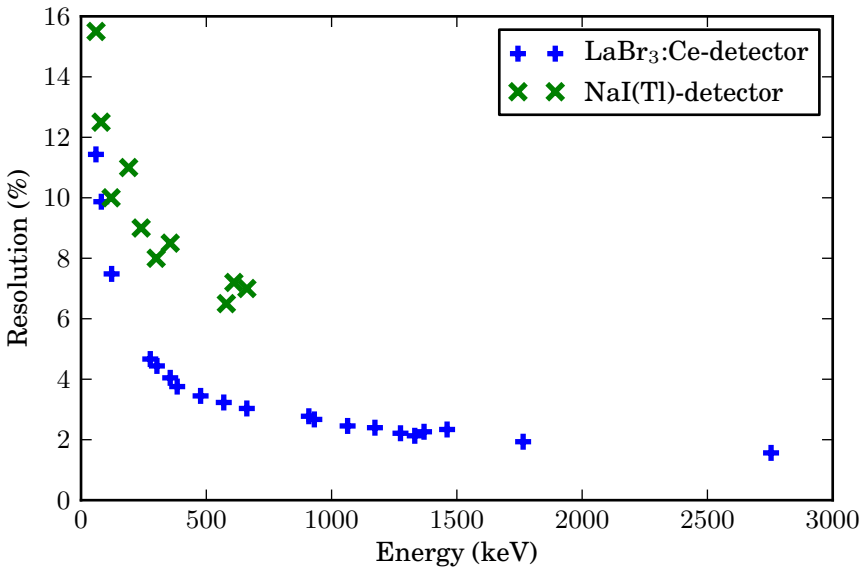

Figure 25: Resolution of the $LaBr_3$:Ce-detector as well as a NaI(Tl)-detector [19].

4.9 Measuring the internal contamination with a NaI(Tl)-detector

The background measurement can be seen together with the measurement of the $LaBr_3$:Ce-crystal in Figure 26.

Although the expected γ-photon energies from the decay of ^{138}La can be seen in the figure, the addition of these peaks only resulted in an additional ~ 6 cps. This addition is more than an order of magnitude less then when measuring normal background radiation with a NaI(Tl)-detector, as normal background radiation induces in the order of 200-500 cps. This leads to the conclusion that if a NaI(Tl)-detector is to be used in close proximity to $LaBr_3$:Ce-detector, for example in a directional γ-spectrometry system, the internal contamination of the $LaBr_3$:Ce-detector will not pose a problem.

4.10 Sensitivity of the $LaBr_3$:Ce-detector in mobile γ-spectrometry

The result which shows the detection limit in γ-photons fluence through the whole detector for 1 second measurements as a function of energy, can be studied in Figure 27.

The figure clearly demonstrates how the increase in resolution increases the sensitivity of the $LaBr_3$:Ce-detector in comparison to NaI(Tl)-detectors at low energies and medium pulse rates. It can also be inferred from Equation (7) that

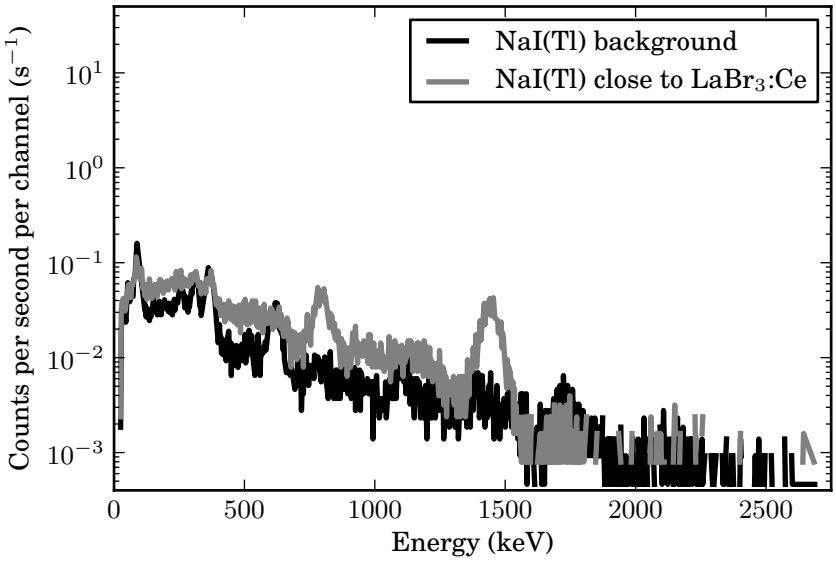

Figure 26: A background measurement in a low-activity environment made with a NaI(Tl)-detector compared to a measurement made in the same environment and the same detector but with a $LaBr_3$:Ce-detector placed beside it.

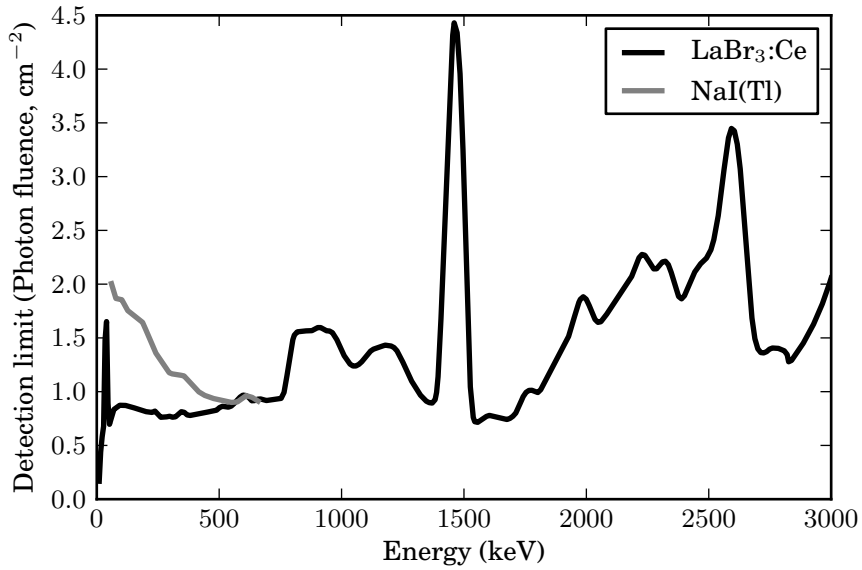

Figure 27: Detection limit comparison between two 3" x 3" detectors. Calculated with the method described in Section 3.10.

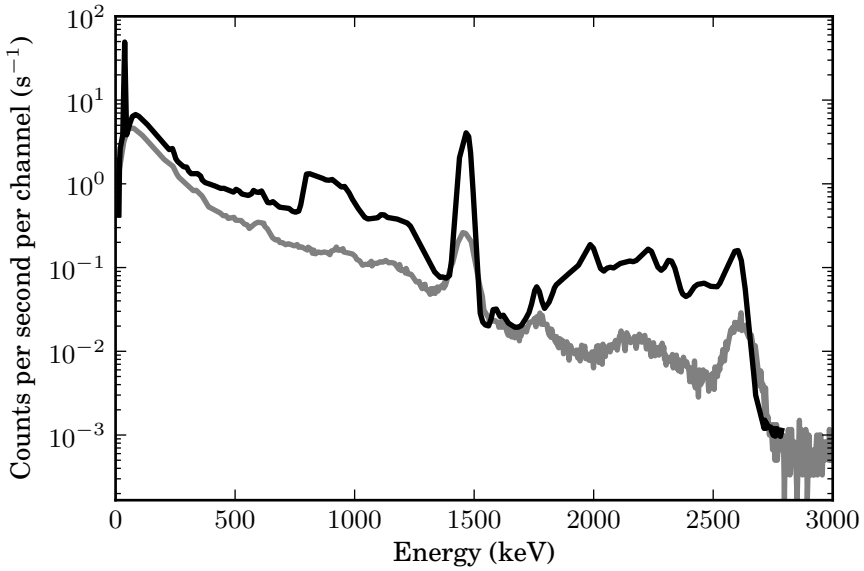

Figure 28: A measurement of naturally occurring γ-radiation. Done with a $LaBr_3$:Ce and a NaI(Tl)-detector.

regardless of resolution, the NaI(Tl)-detector should have a clear advantage in very low pulse rates as the internal contamination of the $LaBr_3$:Ce-detector will drown out other signals in those conditions. There is an indication of this in the figure: Generally, as energy increase, the photon fluence from background radiation at that energy decreases as can be seen in Figure 19. This is not as clear in a $LaBr_3$:Ce pulse height distribution as in NaI(Tl) pulse height distribution because of the internal contamination. For this reason, NaI(Tl)-detectors should have a clear advantage over $LaBr_3$:Ce-detectors in detection limit at high γ-photon energies, even in environments with relatively high background pulse rates. As the pulse rate increases however, and the internal contamination becomes less relevant in the pulse height distribution, the superior resolution of the $LaBr_3$:Ce-detector should make it the better choice.

Usage of resolution data from Milbrath *et al.* [19], though not optimal, should suffice for this comparison. As the resolution data is used in the calculation to obtain the number of background pulses in the pulse height distribution, it is expected that resolution measurements from different NaI(Tl)-detectors should affect the final result of the calculation at most a few percent.

4.11 Comparison of $LaBr_3$:Ce and NaI(Tl) detector measuring background radiation

Figure 28 shows pulses height distribution of the background radiation in an everyday environment. Although the internal background represents a clear ma-

jority (500 of the total 890 cps) of the total amount of pulses in the measurement, the increased resolution over the NaI(Tl)-detector gives the $LaBr_3$:Ce-detector an edge in identifying naturally occurring radiation. As the measurement time was several hours, a background correction would have eased the job of identifying nuclides.

When comparing the waterfall display (Figure 29) from the $LaBr_3$:Ce-detector and the NaI(Tl)-detector, it appears at first glance, that it is easier to spot the ^{137}Cs-source when using the NaI(Tl)-detector. The reason for this is twofold:

- The intensity of the X-ray peak in the $LaBr_3$:Ce waterfall display (Figure 29) masks the intensity of the ^{137}Cs-peak in that diagram. If the X-ray peak were to be removed, the ^{137}Cs-peak would be much more obvious.
- The scattered radiation in the NaI(Tl)-diagram is a great clue to the fact that a source is present. This relatively high percentage of scattered radiation in the waterfall display from the NaI(Tl)-detector is actually a detriment to finding the real peak. This is especially true for γ-peaks at lower energy where the scattered radiation and the full energy peak is closer to each other. The corresponding peak from the $LaBr_3$:Ce-detector however, shows a relatively well defined peak.

The conclusion is that the increased resolution of the $LaBr_3$:Ce-detector makes it superior in this case if the always present internal contamination peaks can be compensated for.

The deviation display shown in Figure 30 accomplishes that which was asked for in the previous sentence. From internal contamination always present structures in the pulse height distribution are mostly removed. This leads to more obvious indicators of the ^{137}Cs-source in both deviation displays. Although it might seem that the structure is more visible in the NaI(Tl)-diagram, the high intensity peak is more well defined in the $LaBr_3$:Ce deviation display. This simplifies the creation of an algorithm which locates radioactive sources.

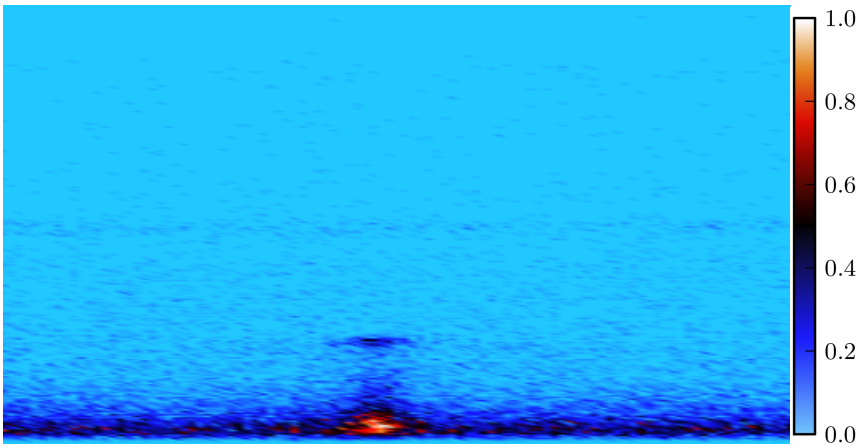

(a) NaI(Tl)-detector

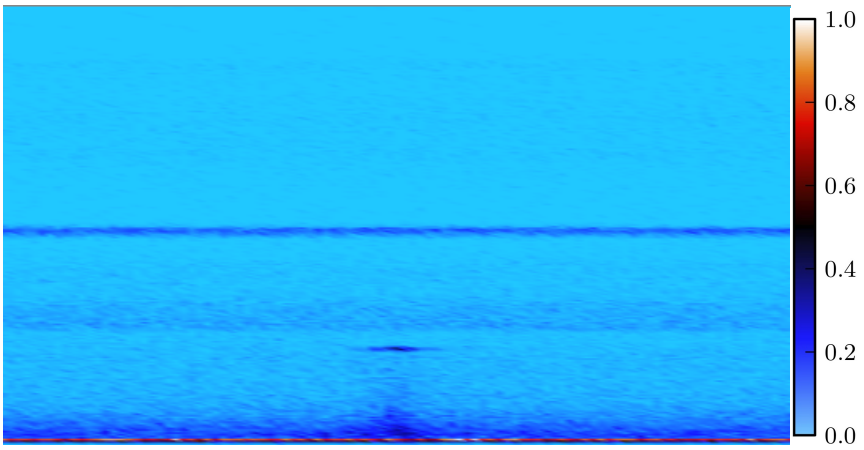

(b) $LaBr_3$:Ce-detector

Figure 29: Waterfall display from a (a) NaI(Tl)-detector and a (b) $LaBr_3$:Ce-detector showing a ^{137}Cs point source. The x-axis is time, the y-axis energy and the colour coding represents intensity. The source had an activity of $\sim$ 37 MBq and was placed 10-20 meters away from a car driving past it at $\sim$35 km/h. Measurement time was 1 second. The ^{138}La/^{40}K-multiplet around 1460 keV is clearly visible in Figure (b). It is also possible to see a hint of the β-continuum and the peaks from the the α-nuclides above and below the ^{138}La/^{40}K-multiplet.

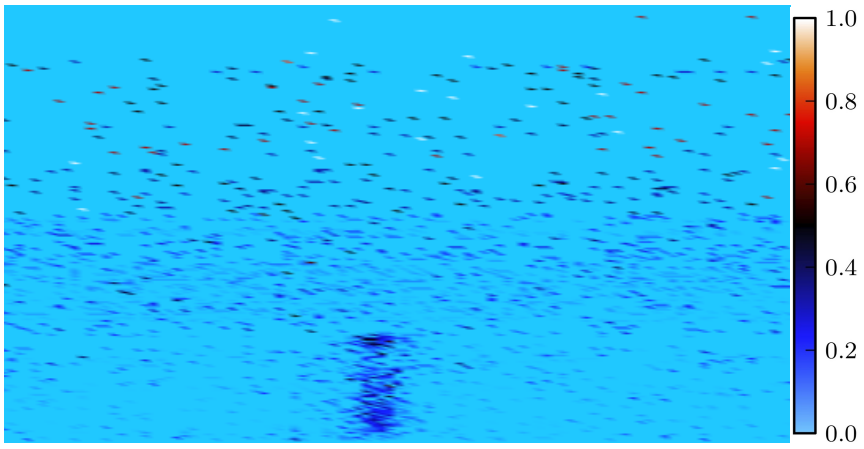

(a) NaI(Tl)-detector

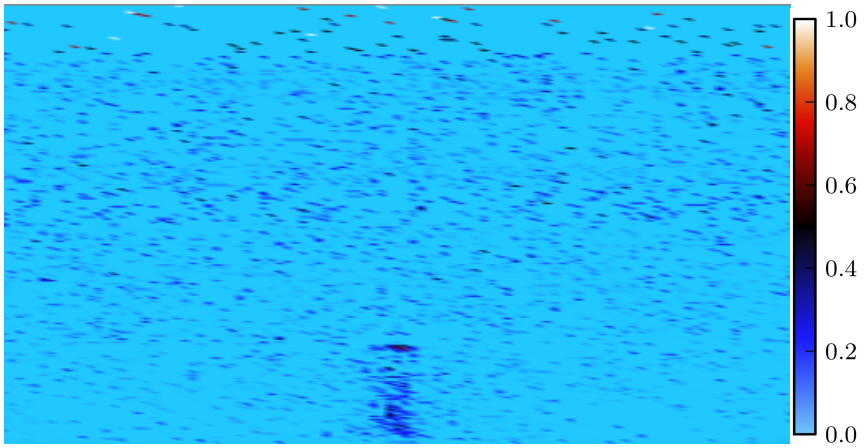

(b) $LaBr_3$:Ce-detector

Figure 30: Deviation display of the data shown in Figure 29. Note that in the "waterfall" display always present structures such as the α-peaks, the $^{138}La/^{40}K$-multiplet around 1460 keV and the β-continuum are not present in the deviation display.

5 Conclusion

The $LaBr_3$:Ce-detector has many qualities that makes it superior to a NaI(Tl)-detector of similar size, such as better resolution and efficiency. Even so, the internal contamination has proved to be the main limiting factor when comparing the two detector types. The conclusion drawn from the work described in this thesis, is that in very low pulse rate environments, the NaI(Tl)-detector is still the superior choice. In medium pulse rate environments however, the increase in resolution over the NaI(Tl)-detector enables the $LaBr_3$:Ce-detector to successfully compete in some energy ranges. Finally, at high pulse rates, the $LaBr_3$:Ce-detector should be very useful as the internal contamination is then negligible in comparison.

Some knowledge of the internal contamination of the $LaBr_3$:Ce-detector must exist when analysing pulse height distributions from that detector, as this enables the separation of peaks and structures from the internal contamination. Though it is possible to subtract the internal contamination from a pulse height distribution, this represents a problem caused by energy calibration drift in the detector caused by temperature change, pulse rate, as well as intrinsic drift. A background subtraction method which compensates for this drift as well as energy resolution drift was tested. It is based on making a model of the internal contamination. This model is constructed out of gaussians with widths representing the energy resolution of the detector at that energy.

If a background correction based on the method above is to be used, good data of the detector linearity, energy calibration and resolution must exist. This holds true for every measurement which is to be made with the detector. This nuisance is compounded by the energy calibration drift that the detector undergoes. There are at least four factors causing energy calibration drift: intrinsic, temperature change, pulse rate change and a change in the magnetic field (i.e. earths magnetic field). Three of these four factors can relatively easily be compensated for by using a stabilisation function. The effect of the earths magnetic field is a more severe problem and the solution here, is likely to make better use of magnetic field shielding materials such as mu-metal.

Another promising way of compensating for the internal contamination, specifically when doing mobile γ-spectrometry, is by using a deviation display which shows changes in the pulse height distribution. As the internal contamination is static in comparison to mobile measurements, this effectively removes all peaks and structures caused by the internal contamination from the deviation display. Using the deviation display makes the $LaBr_3$:Ce-detector reasonably well suited for car or human-borne γ-radiation surveys.

The normal method for stabilising the energy calibration, which is based on ensuring that a peak in a pulse width distribution does not move, is not applicable for the $LaBr_3$:Ce-detector. The reason for this is that the only usable naturally occurring peaks are partly or mostly hidden by the internal contamination. An energy calibration stabilisation method used with the $LaBr_3$:Ce-detector should also take the internal contamination into account.

Acknowledgements

First and most importantly, I would like to thank my supervisors: Robert, Peder and Christer for providing insight and discussions into the experiments performed and the results achieved. I would also like to give a special thank you to Karl Östlund for coming up with suggestions on how to perform some experiments.

Furthermore, Lennart Bergqvist, Inga Göransson, Mats Hansson, Fredrik Henricsson, Gertie Johansson and Jonathan Siikanen have my gratitude for helping me with equipment and providing me with radioactive sources.

I would also like to thank Mattias Jönsson, Jimmy Heimdal and Elna Nilsson for proof-reading the thesis and coming with suggestions on how it could be improved.

Finally, I must thank the Swedish Radiation Safety Authority as this work would not exist without their financing.

References

[1] R. Hofstadter, "Alkali halide scintillation counters," *Phys. Review*, vol. 74, no. 1, pp. 100–101, 1948.

[2] S. Johansson, "Measurements of the energy of beta-and gamma-rays with a scintillation counter," *Nature*, vol. 165, p. 396, Mar 1950.

[3] G. F. Knoll, *Radiation Detection and Measurement*. John Wiley and Sons, Inc., third ed., 1999.

[4] M. Moszyński, "Inorganic scintillation detectors in -ray spectrometry," *Nucl. Instr. and Meth. in Phys. Res., A*, vol. 505, no. 1-2, pp. 101–110, 2003.

[5] E. V. D. van Loef, P. Dorenbos, C. W. E. van Eijk, K. Krämer, and H. U. Güdel, "High-energy-resolution scintillator: Ce^{3+} activated $LaBr_3$," *Appl. Phys. Letters*, vol. 79, pp. 1573–1575, Sep 2001.

[6] J. D. Laeter, J. Bohlke, P. D. Bievre, H. Hidaka, H. Peiser, K. Rosman, and P. Taylor, "Atomic weights of the elements: Review 2000 - (iupac technical report)," *Pure. Appl. Chem.*, vol. 75, pp. 683–800, Jan 2003.

[7] E. Sakai, "Recent measurements on scintillator-photodetector systems," *IEEE Trans. on Nucl. Sci.*, 1987.

[8] K. Shah, J. Glodo, M. Klugerman, W. Moses, S. Derenzo, and M. Weber, "$LaBr_3$:Ce scintillators for gamma ray spectroscopy," *Lawrence Berkeley National Laboratory: Lawrence Berkeley National Laboratory. Retrieved from: http://www. escholarship. org/uc/item/38f0c7zv*, 2002.

[9] J. Glodo, W. Moses, W. Higgins, E. van Loef, P. Wong, S. Derenzo, M. Weber, and K. Shah, "Effects of ce concentration on scintillation properties of $LaBr_3$: Ce," *IEEE Trans. on Nucl. Sci.*, vol. 52, pp. 1805–1808, Jan 2005.

[10] J. S. Schweitzer and W. Ziehl, "Temperature dependence of NaI(Tl) decay constant," *IEEE Trans. on Nucl. Sci.*, vol. 30, pp. 380–382, Apr 1983.

[11] M. Moszyński, A. Nassalski, A. Syntfeld-Każuch, T. Szczęśniak, W. Czarnacki, D. Wolski, G. Pausch, and J. Stein, "Temperature dependences of $LaBr_3$ (Ce), $LaCl_3$ (Ce) and NaI (Tl) scintillators," *Nucl. Inst. and Meth. in Phys. Res., A*, vol. 568, no. 2, pp. 739–751, 2006.

[12] G. Bizarri, J. D. Haas, P. Dorenbos, and C. van Eijk, "First time measurement of gamma-ray excited $LaBr_3$: 5% Ce^{3+} and $LaCl_3$: 10% Ce^{3+} temperature dependent properties," *Physica Status Solidi Appl. Res.*, vol. 203, pp. 41–43, 2006.

[13] H. Toivonen, K. Vesterbacka, A. Pelikan, A. Mattila, and T. Karhunen, "$LaBr_3$ spectrometry for environmental monitoring," *The 12th International Congress of the International Radiation Protection Association*, pp. 1–10, Oct 2008.

[14] P. Menge, G. Gautier, A. Iltis, C. Rozsa, and V. Solovyev, "Performance of large lanthanum bromide scintillators," *Nucl. Inst. and Meth. in Phys. Res., A*, vol. 579, no. 1, pp. 6–10, 2007.

[15] W. Kernan, "Self-activity in lanthanum halides," *2004 IEEE Nucl. Sci. Symp. Conference Record*, vol. 2, 2004.

[16] R. Nicolini, F. Camera, N. Blasi, S. Brambilla, R. Bassini, C. Boiano, A. Bracco, F. Crespi, O. Wieland, and G. Benzoni, "Investigation of the properties of a 1" x 1" $LaBr_3$: Ce scintillator," *Nucl. Inst. and Meth. in Phys. Res., A*, vol. 582, no. 2, pp. 554–561, 2007.

[17] B. Milbrath, R. Runkle, T. Hossbach, W. Kaye, E. Lepel, B. McDonald, and L. Smith, "Characterization of alpha contamination in lanthanum trichloride scintillators using coincidence measurements," *Nucl. Inst. and Meth. in Phys. Res., A*, vol. 547, no. 2-3, pp. 504–510, 2005.

[18] K. Alzimami, E. Abuelhia, Z. Podolyak, A. Ioannou, and N. Spyrou, "Characterization of $LaBr_3$: Ce and $LaCl_3$: Ce scintillators for gamma-ray spectroscopy," *J. of Radioanalytical and Nucl. Chem.*, vol. 278, no. 3, pp. 755–759, 2008.

[19] B. D. Milbrath, B. J. Choate, J. E. Fast, W. K. Hensley, R. T. Kouzes, and J. E. Schweppe, "Comparison of $LaBr_3$: Ce and NaI(Tl) scintillators for radio-isotope identification devices," *Nucl. Instr. and Meth. A*, vol. 572, pp. 774–784, Jan 2007.

[20] P. Dorenbos, J. D. Haas, and C. van Eijk, "Gamma ray spectroscopy with a $\varnothing$19 x 19 mm^3 $LaBr_3$: 0.5% Ce^{3+} scintillator," *IEEE Trans. on Nucl. Sci.*, vol. 51, pp. 1289–1296, Jan 2004.

[21] M. Balcerzyk, M. Moszyński, and M. Kapusta, "Comparison of $LaCl_3$: Ce and NaI(Tl) scintillators in gamma-ray spectrometry," *Nucl. Instr. and Meth. A*, vol. 537, pp. 50–56, Jan 2005.

[22] R. Pani, M. N. Cinti, R. Scafè, R. Pellegrini, F. Vittorini, P. Bennati, S. Ridolfi, S. L. Meo, M. Mattioli, G. Baldazzi, F. Pisacane, F. Navarria, G. Moschini, P. Boccaccio, V. O. Cencelli, and D. Sacco, "Energy resolution measurements of $LaBr_3$:Ce scintillating crystals with an ultra-high quantum efficiency photomultiplier tube," *Nucl. Inst. and Meth. in Phys. Res., A*, vol. 610, pp. 41–44, Nov 2009.

[23] F. Quarati, A. Bos, S. Brandenburg, C. Dathy, P. Dorenbos, S. Kraft, R. Ostendorf, V. Ouspenski, and A. Owens, "X-ray and gamma-ray response of a 2" x 2" $LaBr_3$: Ce scintillation detector," *Nucl. Inst. and Meth. in Phys. Res., A*, vol. 574, no. 1, pp. 115–120, 2007.

[24] R. J. Barlow, *Statistics: A Guide to the Use of Statistical Methods in the Physical Sciences*. John Wiley and Sons, Inc., 1989.

[25] K. S. Krane, *Introductory nuclear physics*. John Wiley and Sons, Inc., 1987.

[26] L. Currie, "Limits for qualitative detection and quantitative determination. application to radiochemistry," *Analytical Chem.*, vol. 40, no. 3, pp. 586–593, 1968.

[27] R. Fink, "Field gamma-ray spectrometry: Theory of calibration and measurement using germanium spectrometer," 1992.

[28] H. Toivonen May 2010. Personal communication.

[29] Saint-Gobain Crystals, *SGC BrilLanCe Scintillators Performance Summary*, Jan 2009.

[30] G. Meinrath, C. Ekberg, A. Landgren, and J. Liljenzin, "Assessment of uncertainty in parameter evaluation and prediction," *Talanta*, vol. 51, no. 2, pp. 231–246, 2000.

[31] A. Hindmarsh, "Lsode and lsodi, two new initial value ordinary differnetial equation solvers," *ACM SIGNUM Newsletter*, vol. 15, pp. 10–11, Dec 1980.

[32] P. Kock, R. R. Finck, J. M. C. Nilsson, K. Östlund, and C. Samuelsson, "A deviation display method for visualising data in mobile gamma-ray spectrometry," *Appl. Radiation and Isotopes*, vol. 68, pp. 1832–1838, May 2010.

[33] W. Higgins, J. Glodo, E. van Loef, M. Klugerman, T. Gupta, L. Cirignano, P. Wong, and K. Shah, "Bridgman growth of $LaBr_3$: Ce and $LaCl_3$: Ce crystals for high-resolution gamma-ray spectrometers," Jan 2006.

A Populärvetenskaplig samanfattning

Det finns i huvudsak tre typer av joniserande strålning[3]: alfa, beta och gamma. Alfa och beta-strålning har relativt begränsad räckvidd medan gamma-strålning (γ-strålning) generellt sett har längst räckvidd av de tre. γ-strålning är i princip samma typ av strålning som synligt ljus, med enda skillnaden att energin i γ-strålning är ofantligt mycket högre än energin i vanligt ljus. För att kunna mäta hur hög energin är, så har man sen 1950-talet använt detektorer av typen natriumjodid (NaI). NaI-detektorer är en typ av detektorer som tillhör gruppen scintillationsdetektorer eftersom de skickar ut en kort ljuspuls när de träffas av γ-strålning. Denna ljuspuls kan utläsas för att ta reda på energin hos den γ-strålningen som träffade detektorn.

Nackdelarna med NaI-detektorn är dock många: Den har dålig upplösning vilket betyder att den har svårt att särskilja γ-energier som ligger nära varandra. Den är också känslig för temperaturförändringar.

För att lösa dessa problem (med flera), så utvecklades för några år sedan en ny typ av scintillator-detektor som heter lantaniumbromid (LaBr). Denna detektor har bättre upplösning än NaI-detektorn men är också känsligare för γ-strålning och har ett antal andra egenskaper som gör den bättre än NaI-detektorer. Den har dock en stor nackdel: LaBr-detektorn är radioaktiv i sig själv.

LaBr-detektorns radioaktivitet betyder att var och hur man än mäter så kommer man alltid att mäta radioaktivitet som kommer från detektorn själv: Detta är förstås ett problem, speciellt när man ska mäta γ-strålning från väldigt svagt radioaktiva källor.

Det här arbetet har bland annat gått ut på att försöka hitta metoder för att kompensera för den radioaktive föroreningen i LaBr-detektorer. En metod som provades var att skapa en modell av hur den interna radioaktiviteten påverkar mätningarna och med hjälp av denna modell, justera resultatet. Andra frågor som har studerats är exempelvis hur olika temperaturer påverkar hur detektorn fungerar och huruvida det går att använda LaBr-detektorn vid mätningar ute i naturen istället för att bara använda den i laboratorier.

[3] I folkmun det felaktiga uttrycket "radioaktiv strålning".